

**DAHLGREN DIVISION  
NAVAL SURFACE WARFARE CENTER**

Dahlgren, Virginia 22448-5100



**NSWCDD/TR-95/18**

**WIDEBAND LOW ELEVATION MICROWAVE  
PROPAGATION MEASUREMENTS**

**BY JAMES L. QUEEN    JANET STAPLETON    STEVEN KANG**  
**SHIP DEFENSE SYSTEMS DEPARTMENT**



**FEBRUARY 1995**

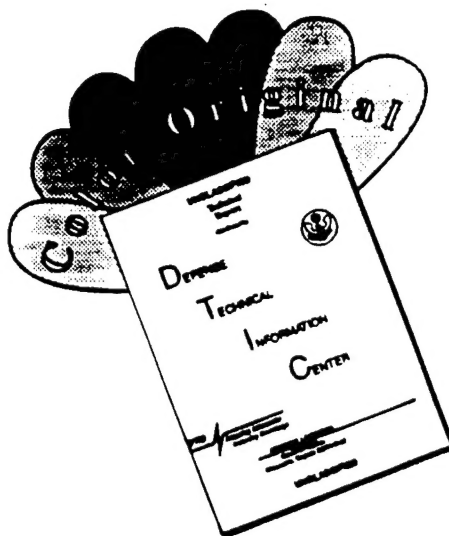
Approved for public release, distribution is unlimited.

*DTIC ELECTE stamp*  
All DTIC reproduction  
must be in black and  
white.

**19951103 058**

**DTIC QUALITY INSPECTED 1**

# DISCLAIMER NOTICE

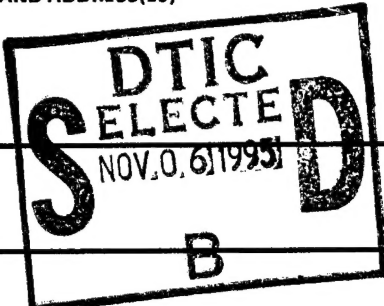
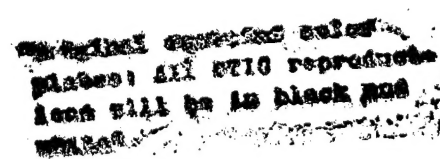


THIS DOCUMENT IS BEST QUALITY AVAILABLE. THE COPY FURNISHED TO DTIC CONTAINED A SIGNIFICANT NUMBER OF COLOR PAGES WHICH DO NOT REPRODUCE LEGIBLY ON BLACK AND WHITE MICROFICHE.

# REPORT DOCUMENTATION PAGE

Form Approved  
OMB No. 0704-0188

Public reporting burden for this collection of information is estimated to average 1 hour per response, including the time for reviewing instructions, searching existing data sources, gathering and maintaining the data needed, and completing and reviewing the collection of information. Send comments regarding this burden estimate or any other aspect of this collection of information, including suggestions for reducing this burden, to Washington Headquarters Services, Directorate for Information Operations and Reports, 1215 Jefferson Davis Highway, Suite 1204, Arlington, VA 22202-4302, and to the Office of Management and Budget, Paperwork Reduction Project (0704-0188), Washington, DC 20503.

<b>1. AGENCY USE ONLY (Leave blank)</b>		<b>2. REPORT DATE</b> February 1995	<b>3. REPORT TYPE AND DATES COVERED</b> Final	
<b>4. TITLE AND SUBTITLE</b> Wideband Low Elevation Microwave Propagation Measurements			<b>5. FUNDING NUMBERS</b>	
<b>6. AUTHOR(S)</b> J. Queen, J. Stapleton, S. Kang				
<b>7. PERFORMING ORGANIZATION NAME(S) AND ADDRESS(ES)</b> Naval Surface Warfare Center Dahlgren Division, F42 17320 Dahlgren Road Dahlgren, VA 22448-5100			<b>8. PERFORMING ORGANIZATION REPORT NUMBER</b> NSWCDD/TR-95/18	
<b>9. SPONSORING/MONITORING AGENCY NAME(S) AND ADDRESS(ES)</b>			<b>10. SPONSORING/MONITORING AGENCY REPORT NUMBER</b>	
<b>11. SUPPLEMENTARY NOTES</b>				
<b>12a. DISTRIBUTION/AVAILABILITY</b>  Approved for public release, distribution is unlimited.			<b>12b. DISTRIBUTION CODE</b>	
<b>13. ABSTRACT (Maximum 200 words)</b>  A system is described that directly measures microwave propagation loss at low altitudes through the transmission of radio frequency signals. The system is designed to collect pathloss data over a 2 to 18 GHz band to better understand the phenomena that affect the detection of low altitude targets by radars operating in a maritime environment. Data were collected between January and April 1994 as part of the Multisensor Integration Tests held at the Naval Surface Warfare Center, Wallops Island Detachment. Detailed analysis is performed on a subset of the data; illustrations provided show the temporal and spatial character of the propagation.   				
<b>14. SUBJECT TERMS</b> low altitude, radar propagation, Multisensor Integration Tests, refractive index, transmitter, receiver, antenna, calibration, YIG Filter, meteorological data, ducting, subrefraction, null variability, RF path loss, 2 to 18 GHz, temporal and spatial loss variability, frequency line plot, static plot, dynamic plot			<b>15. NUMBER OF PAGES</b> 88	
			<b>16. PRICE CODE</b>	
<b>17. SECURITY CLASSIFICATION OF REPORT</b> UNCLASSIFIED	<b>18. SECURITY CLASSIFICATION OF THIS PAGE</b> UNCLASSIFIED	<b>19. SECURITY CLASSIFICATION OF ABSTRACT</b> UNCLASSIFIED	<b>20. LIMITATION OF ABSTRACT</b> UL	

## FOREWORD

This report is a summary of the equipment used, test scenarios followed, types of data collected and general conclusions reached regarding radio frequency (RF) propagation measurements that were part of the Multi-Sensor Integration Tests conducted by the Naval Surface Warfare Center, Dahlgren Division (NSWCDD) at Wallops Island, December 1993 to April 1994. For the first time, RF propagation structure has been measured and recorded at a high sampling rate, across a broad frequency span simultaneously for a mix of heights at two terminals, and for a wide range of propagation conditions. For the data collected, the mid-frequency range was favored (6 to 12 GHz); the benefits of radar height diversity were evident; small-scale changes in target height (3 ft or less) were shown to be responsible for large (15 dB one-way) variations in pathloss; significant changes were measured in these loss structures in a period of less than 20 sec, especially during strong ducting. Comparisons of the measured pathloss data with models of propagation fed by meteorological measurements of refractivity showed some large-scale agreement in character, but often missed the mark on a more detailed scale. Only a portion of the data collected is included in this report, but these data are representative of events from the entire test period. Related measurements made using a single-frequency Ku-band propagation measurement system, which measured patterns across range, are covered in NSWCDD technical report TR-95/66. A similar report (TR-95/33) has been generated as a summary of the infrared (IR) propagation measurements that were conducted jointly with the RF propagation measurements during the test period. A combined IR/RF propagation analysis is in process including joint performance information as it applies to multi-sensor integration. A report of the IR/RF propagation analysis will be published as NSWCDD technical report TR-95/60.

As stated, the collection of the data contained in this report is unique in terms of the bandwidth covered and sampling rate for the low elevation region, and would not have been possible without the efforts of an extremely talented and dedicated engineering team. Through their efforts in negotiating with the Nature Conservancy for the use of Parramore Island, Mr. Charles Traylor and Mr. G. Mike Turman were instrumental in making possible the remote site where the transmitters were located. Mr. Traylor and Mr. Turman were also responsible for the engineering design and development of the power generation unit and support structures and for the physical movement of equipment and fuel to and from Parramore Island. METRATEK INC. was responsible for hardware fabrication control, software development, and system integration. METRATEK worked closely with NSWCDD on the engineering design of the system. The microwave propagation test team included Steve Kang (F42), Jim Queen (F05), Janet Stapleton (F42), Stan Vandruff (F41), and Mike Campbell of PRC. Meteorological data were collected by Ralph Dickerson (F41), and by Dan Dockery, John Rowland and Jim Meyer of the Applied Physics Lab. Additional personnel who helped during the initial setup of the equipment included Gary Bass (G541), Jimmy Clarke (G541), Darryl Matthews (G541), and Joe Minter (F41).

on For	
RA&I	
B	
aced	
cation	
Distribution/	
Availability Codes	
Dist	Avail and/or
A-1	Special



This report was reviewed by E.A. Hodgson, Head, AN/SPY-1 System Branch, and S.A. Koch, Head, Search and Track Division.

Approved by:

A handwritten signature in black ink, appearing to read "Thomas C. Pendergraft", with a stylized flourish at the end.

THOMAS C PENDERGRAFT, Head  
Ship Defense Systems Department

## CONTENTS

<u>Section</u>	<u>Page</u>
1 INTRODUCTION .....	1-1
2 EQUIPMENT AND TEST DESCRIPTIONS .....	2-1
MICROWAVE PROPAGATION MEASUREMENT SYSTEM .....	2-1
MAJOR FEATURES OF THE SYSTEM .....	2-4
ACCURACY .....	2-8
3 METEOROLOGICAL DATA COLLECTED .....	3-1
METEOROLOGIC (MET) VAN .....	3-1
100-FT METEOROLOGICAL POLE (10-SENSOR ARRAY) .....	3-1
100-FT METEOROLOGICAL TOWER (SINGLE SENSOR), Y85 .....	3-2
APPLIED PHYSICS LABORATORY (APL) METEOROLOGICAL SUPPORT .....	3-2
NASA GROUND STATION METEOROLOGICAL DATA .....	3-3
IR RADIATION METEOROLOGICAL BUOY .....	3-3
4 TEST RESULTS .....	4-1
TRANSITION FROM DUCTING TO SUBREFRACTION .....	4-1
RECEIVER HEIGHT EFFECTS DURING DUCTING .....	4-11
VERTICAL NULL VARIABILITY .....	4-16
FREQUENCY EFFECTS ON NULL FILLING .....	4-32
5 SUMMARY AND GENERAL OBSERVATIONS .....	5-1
FREQUENCY .....	5-1
RECEIVER HEIGHT .....	5-1
TRANSMITTER HEIGHT .....	5-2
TEMPORAL VARIABILITY .....	5-2
METEOROLOGICAL DATA AND MODEL PREDICTIONS .....	5-2
DUCTING ENVIRONMENT .....	5-3
6 FUTURE MEASUREMENTS .....	6-1
7 CONCLUSIONS .....	7-1
8 REFERENCES .....	8-1

**CONTENTS (Continued)**

<u>Section</u>	<u>Page</u>
APPENDIX A-EQUIPMENT DESCRIPTION .....	A-1
DISTRIBUTION .....	(1)

## ILLUSTRATIONS

<u>Figure</u>		<u>Page</u>
2-1	MPMS DATA COLLECTION PATH .....	2-2
2-2	TEST EQUIPMENT CONFIGURATION .....	2-3
4-1	FREQUENCY LINE PLOT 24 MAR 94 05:31 UTC .....	4-2
4-2	FREQUENCY LINE PLOT 24 MAR 94 06:21 UTC .....	4-3
4-3	FREQUENCY LINE PLOT 24 MAR 94 06:51 UTC .....	4-5
4-4	FREQUENCY LINE PLOT 24 MAR 94 06:51 UTC, 4/3 EARTH REFERENCE .....	4-7
4-5	FREQUENCY LINE PLOT 24 MAR 94 08:11 UTC .....	4-9
4-6	STATIC PLOT 22 MAR 94 14:38 UTC .....	4-12
4-7	STATIC PLOT 23 MAR 94 13:49 UTC .....	4-13
4-8	MODEL OUTPUT 23 MAR 94 RUN 1 PROFILE 1 .....	4-15
4-9	MODEL OUTPUT 22 MAR 94 RUN 2 PROFILE 1 .....	4-17
4-10	REFRACTIVE PROFILE 23 MAR 94 RUN 1 PROFILE 1 .....	4-18
4-11	REFRACTIVE PROFILE 22 MAR 94 RUN 2 PROFILE 1 .....	4-19
4-12	DYNAMIC PLOT 23 MAR 94 07:01 UTC .....	4-20
4-13	LINE PLOT, 3.6 GHZ, 23 MAR 94 07:01 UTC .....	4-21
4-14	LINE PLOT, 8.475 GHZ, 23 MAR 94 07:01 UTC .....	4-22
4-15	LINE PLOT, 15.0 GHZ, 23 MAR 94 07:01 UTC .....	4-23
4-16	DYNAMIC PLOT 23 MAR 94 07:33 UTC .....	4-25
4-17	DYNAMIC PLOT 22 MAR 94 19:54 UTC .....	4-27
4-18	MODEL OUTPUT 22 MAR 94 RUN 5 PROFILE 1 .....	4-29
4-19	REFRACTIVE PROFILE 22 MAR 94 RUN 5 PROFILE 1 .....	4-30
4-20	DYNAMIC PLOT 22 MAR 94 22:44 UTC .....	4-31
4-21	LINE PLOT 23 MAR 94 07:04 UTC; 5.9, 8.475, 13.57, 17.35 GHZ .....	4-33

## TABLES

<u>Table</u>		<u>Page</u>
2-1	MPMS PERFORMANCE, SIGNAL-TO-NOISE RATIO .....	2-8
2-2	RECEIVER 1 CALIBRATION DATA .....	2-9
2-3	TRANSMITTER 8 CALIBRATION DATA .....	2-10
2-4	ANTENNA GAIN .....	2-13
2-5	SYSTEM ACCURACY .....	2-14

**GLOSSARY**

A/D	Analog-to-Digital
FFT	Fast Fourier Transform
GPS	Global Positioning System
I	In-phase
IF	Intermediate Frequency
IR	Infrared
LO	Local Oscillator
MET	Meteorologic
MPMS	Microwave Propagation Measurement System
MSI	Multisensor Integration
NASA	National Aviation and Space Administration
NSWCDD	Naval Surface Warfare Center, Dahlgren Division
NSWCDL	Naval Surface Warfare Center, Dahlgren Laboratory
PCPEM	Personal Computer Parabolic Equation Model
Q	Quadrature
RF	Radio Frequency
RMS	Root Mean Square
RX	Receiver
SBIR	Small Business Innovative Research
TX	Transmitter
UTC	Universal Time Coordinated
VHF	Very-High Frequency

## SECTION 1

### INTRODUCTION

Radio frequency (RF) propagation at low altitudes is strongly affected by the structure of the refractive index of the lower atmosphere. RF propagation in this region has long been known to vary with altitude, range, time and frequency. Under subrefractive conditions, the radar horizon may be significantly reduced. Under enhanced propagation conditions, deep nulls have been both predicted and observed with widths less than 3 ft in altitude, and having varying, and inadequately defined, temporal and spatial characteristics. Testing of developmental sensor systems in this low altitude region of high variability of propagation is beset with the difficulty of achieving enough test runs over broad environmental conditions to adequately quantify performance. The problem is compounded by the necessity of testing with surrogate targets, which then requires the scaling of results in altitude and range in this most difficult region. As a general rule, in previous analyses of test data, equipment and target parameters were accounted for and whatever was left as deviation from a calculated reference condition was attributed to propagation. Limited supporting propagation measurements may have been made with the sensor, but not usually at the time of the test runs. Further insight into RF propagation was usually sought by executing computer models that used as inputs refractive index profiles (and surface conditions) calculated from measurements of surface and air temperature, relative humidity, pressure, and wind speed. The parabolic equation-based microwave propagation models now becoming generally available are reputed to be, and are believed to be, accurate when adequate profiles are available along the propagation path. However, these refractive profiles are very difficult to acquire, and the process is time-consuming. Further, even with the best of models, the short-term dynamics of propagation are still out of reach. In view of these deficiencies, a task was undertaken to make direct measurements of RF propagation rapidly and simultaneously over multiple one-way paths in the low altitude region critical to the defense of surface ships against low altitude missile attack. Initial goals were to instrument in a form suitable for support of planned land-based-sensor tests at Naval Surface Warfare Center, Dahlgren Laboratory (NSWC DL) and Wallops Island, both to get greater immediate benefit from the tests and to further understanding of propagation in the critical region. Longer range goals were to use the results of the initial tests to determine features that made sense for carrying forward to later at-sea testing and possibly to operational systems.

A mechanization was conceived in which multiple low-power transmitters, at heights typical of low altitude missiles, were used with multiple receivers, at heights typical of shipboard radars. The transmitter set was configured to be carried by a boat for probing in range or for mounting on land at a fixed overwater distance. The receivers were to be land-mounted. The control computers in the transmitter and receiver terminals were connected by radio for control from the receiver end. The transmitters were separated by selected audio-frequency increments from a common carrier so that each receiver could process the height information in parallel by Fast Fourier Transform (FFT) discrimination of the individual transmitter signals. The design that was ultimately accepted allows

for stepping through 16 carrier frequencies anywhere from 2 to 18 GHz at a maximum switching rate of twice per second. Data storage of the appropriate FFT outputs yields a storage requirement amenable to unattended round-the-clock operation. Radar tests with targets are difficult and costly to run at night, but by measuring the propagation at night and also when the radar tests are run, performance may be confidently extrapolated to this period during which propagation transitions often occur.

The system parameters allow spectral space for 2 transmitter arrays (10 transmitters each) to allow probing in frequency, height, and range, with 1 transmitter array along the path to a second transmitter array probing in frequency and height at a fixed range. Cost and time constraints did not permit the implementation of this approach. Instead, the second system was simplified to a single receiver observing a single-frequency transmitter, at 13.95 GHz, scanning in height at one profile per minute. As of the date of this report, the 10-transmitter wideband system has been operated at fixed range separations only. The single-frequency system has been operated in a fixed position and also on the test boat, *Sea Lion*, sometimes measuring along the path to the wideband system and sometimes measuring at other azimuths. Results from the single-frequency system are reported separately.



## SECTION 2

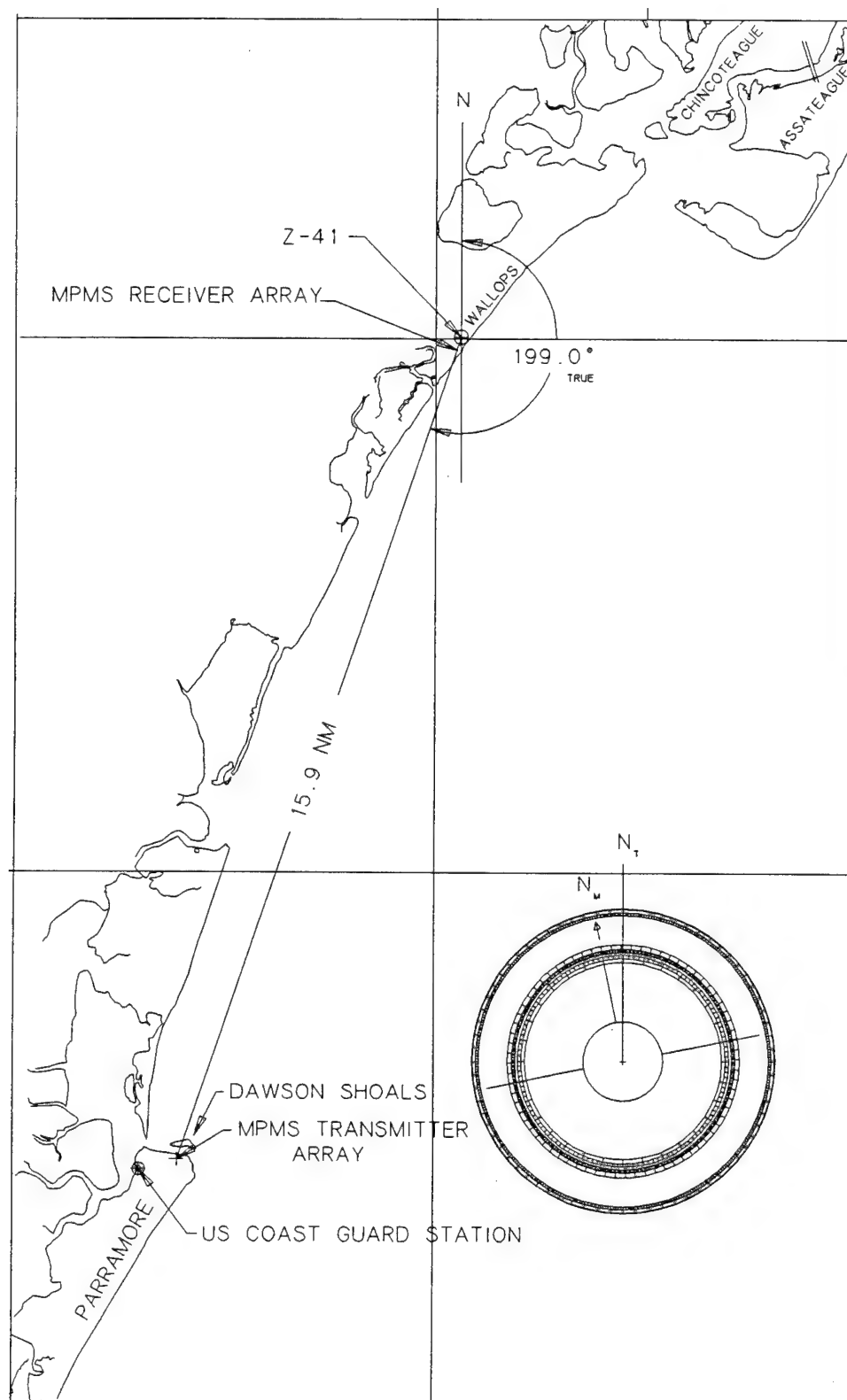
### EQUIPMENT AND TEST DESCRIPTIONS

#### MICROWAVE PROPAGATION MEASUREMENT SYSTEM

General design of the broadband system (known as the Microwave Propagation Measurement System, or MPMS) was initiated in August 1991, building on an approach first broached in 1978. Nearing completion separately in December 1991 was a Small Business Innovative Research (SBIR) Phase I study contract to define a system having similar measurement capability. After designs were compared and further tradeoff studies performed, a Phase II SBIR contract was executed with METRATEK, INC. (12 August 1992) for construction of a broadband system having fewer receivers than originally proposed (4 vice 10) but having broader frequency coverage and greater flexibility (2 to 18 GHz synthesizer with a selectable 16-step pattern vice 4 fixed frequencies). The MPMS was delivered to Dahlgren on 26 August 1993 for onsite acceptance testing. The transmitter system was set up at the edge of the Potomac River at Range Station 21, where shore power was available. The receiver system was set up at the high tide level on the river at the Dahlgren main range with the receivers at the same height, 8 ft above mean water level, and spaced laterally by 3 ft. The site separation distance was 9.875 nmi. The lowest transmitter unit was at a height of 8 ft above mean water level.

In December 1993 the system was moved to Wallops Island, Virginia, where the transmitter system was set up for continuous unmanned operation at Parramore Island. The receiver tower was initially placed at the high tide point on the beach, but prior to operation, a severe storm necessitated partial dismantling and inspired a move to slightly higher ground about 150 ft inland. The site separation between transmitters and receivers was 15.9 nmi and the lowest transmitter was at a height of 7.7 ft above mean sea level. The heights of the receivers were 18.2, 53.3, 68.2, and 83.2 ft above mean sea level. The tests at Wallops Island terminated on 11 April 1994 and the MPMS was returned to Dahlgren and set up as before, but with the receivers on the tower at different heights.

Figure 2-1 shows the path over which the Parramore Island data were taken. Figure 2-2 shows a diagram of the test equipment as it was used during Wallops Island data collection. The "Moving Tx," the boat, the infrared (IR) sources, and the "IR Sensor" shown in Figure 2-2 were used jointly with the MPMS during the tests, but are not discussed in this report. The technical reports listed in the Foreword discuss measurements with these sensors. An overview of system characteristics follows, including descriptions of software modifications installed at various stages. A detailed description of the hardware is contained in Appendix A. The system User's Manual describes operational capabilities in detail.



• FIGURE 2-1. MPMS DATA COLLECTION PATH

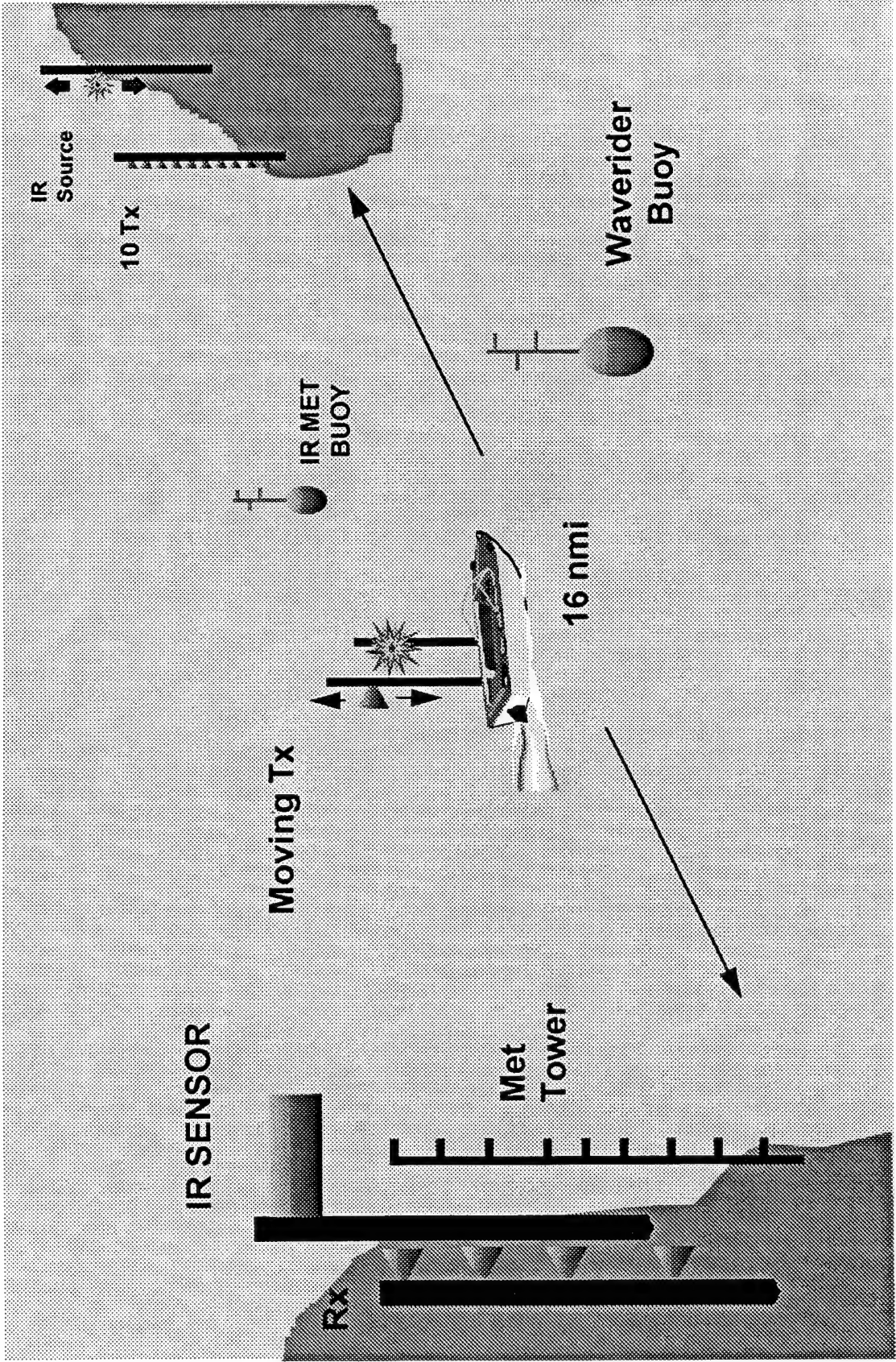


FIGURE 2-2. TEST EQUIPMENT CONFIGURATION

## MAJOR FEATURES OF THE SYSTEM

### Transmitters

The system has 10 transmitters mounted 3 ft apart on a triangular cross-section aluminum tower with antennas coplanar and, usually, vertically polarized. The nominal power supplied to each antenna is 0.1 W and the frequency coverage is 2 to 18 GHz. For normal operation, the tower is vertical with the lowest transmitter less than 10 ft above mean water level. There is an azimuthal adjustment on the tower to set the path direction. The tower is pivoted at a point about 6 ft off the ground and may be rotated for calibration to a horizontal position perpendicular to the measured path direction. Additionally, each antenna may be rotated by 90 deg to realign polarization with the receivers. Transmissions in this configuration may be used for gain normalization since the antenna heights, and subsequent pathloss in this condition, should be the same for all transmitters. The individual transmitter frequencies are offset with respect to one another by differences of 300 Hz to 1 kHz, at the discretion of the operator. The standard offsets were selected to minimize intermodulation components for the system. The output power of each transmitter is monitored frequency-by-frequency as the system switches through the band at rates up to two steps per second (in some modes, four steps per second may be used). In normal operation the power monitor values are communicated to the receiver site for storage and for use in the propagation factor calculation.

### Receivers

The system has four receivers mounted on a 100-ft tower at selected spacing. There is an azimuthal adjustment on the tower to set the path direction. The tower is hinged at 5 ft off the ground and may be rotated to a horizontal position opposite to the path direction for receiver calibration. Because of the wide RF operating band, the receivers have current-controlled YIG preselection filters to protect against interference. The 4-dB loss in the YIGs results in a system noise figure of about 10 dB. Spectral analysis is conducted digitally via an FFT. The amplitudes in the spectral positions of the known 10 transmitted tones are extracted for display and recording. Weighting, padding, and postdetection averaging options are available.

### Antennas

Identical antennas are used in the transmitters and receivers. The gains of one pair of the antennas were measured across 2 to 18 GHz every 0.5 GHz. (The rest were spot-checked at three frequencies.) The averages of the two measured gain values were tabulated and are used in the calculation of propagation factor. Table values are interpolated for actual frequencies selected for use. The tabulation of these antenna gains is included later in Section 2 under "ACCURACY" ("Antenna Gain Accuracy"). The antennas are not included in the transmitter and receiver calibration processes but are, at least as regards the transmitters, in the system calibration.

### Timing, Control, Processing and Recording

The transmitter and receiver systems are both computer-controlled with connection provided by very-high frequency (VHF) packet radio. A precise reference frequency (to support narrow-bandwidth frequency analysis) and precise timing (to support time-commanded operations) are provided at each site by a Global Positioning System (GPS) receiver. Data collection parameters are selected at the receive site and communicated to the transmit site for execution on a specified time basis. The transmit site sends power monitor values before the start of a collection period and periodically during collection so that calibrated data may be observed online. Each receiver switches frequency synchronously with the transmitter set, converts the received signal set to baseband, and takes 4096 In-phase (I) and Quadrature (Q) samples of data at 25 kHz, and at a predetermined interval after transmitter frequency switching. Processing to date has been I or Q only; the complex option is available but not tested. Spurious signal levels were held at least 40 dB below the largest signal. Processing ranges from a single 4096-point transform to transforms of shorter data lengths with zero padding, overlap, and averaging options using part or all of the 4096 signal samples (but not extending beyond the 4096 samples). For example, 512 data samples might be zero-padded to 2048, have a Hanning weight applied, be Fast Fourier Transformed and averaged with 14 other FFT results accruing from shifting by 256 data samples per step for 50 percent data overlap. Data storage is on 8-mm tape with a file per collection interval. Selected peak signal values are recorded along with telemetered transmitter-power-monitor values and other supporting calibration and diagnostic data. A single data tape can record for more than 2 weeks around the clock at half-second switching intervals for an 8-min collection every 10 min. The 2-min dead time is about the minimum that may be used because of data rate limitations in the packet radio telemetry connection.

### Operation with Telemetry Failure

The transmitter site is often remotely located, unmanned, and difficult to reach. To maintain operation in the event of telemetry failure, each site recognizes telemetry failure and switches to a preselected mode. In this event, the transmitter stores power-monitor values on disk for later recovery and correction in an offline processing mode. Online processing uses a default power assumption. The recordings are labeled as not having power-monitor values.

### Calibration

Transmitter Calibration. Individual transmitter calibration is accomplished by rotating the tower to the horizontal position, then connecting a power meter in place of the transmitter antenna and measuring the power-monitor reading versus power-meter reading as power is varied under computer control for each frequency in use. A power intercept and slope is then computed for each frequency.

Receiver Calibration. Individual receiver calibration is accomplished using a calibration box which uses the local oscillator (LO) signal obtained from a tap point to generate a signal offset from the LO by the intermediate frequency (IF) plus 2000 Hz. With the tower down, a receiver is calibrated by first stepping through the frequencies and measuring the power out of the calibration



box, then connecting the calibration box in place of the antenna, setting the internal calibrated attenuator at an appropriate level, and measuring the receiver output power (and hence the receiver gain). During development, YIG tuning characteristics were measured versus temperature and frequency and were used to prepare a table of tuning corrections for each YIG across the band. In system operation, the monitored YIG temperatures were used to keep the system in tune. When the temperature at Wallops Island dropped below the measured region of the table values, performance anomalies were noted and traced to YIG tuning deficiencies. YIG temperature is recorded and the affected data may be excised. Two software changes were effected to remedy the problem. On 14 February 1994, software was introduced that, during receiver calibration, tuned the YIG over 50 MHz centered on applicable table values to guarantee that the peak signal gain was measured. On 18 February 1994, software was installed to produce new tables by disabling the system transmitters, injecting calibration signals locally, and determining the correct tuning offsets for the existing YIG temperatures. On 22 February 1994, the system remained activated through the night in the calibration mode to update the YIG temperature tuning tables. All tables are archived. Further problems were experienced with YIG temperature monitoring until 4 March 1994 when all four channels were repaired and a system calibration conducted.

System Calibration. System calibration, which is in reality system normalization, is accomplished by rotating the transmitter tower to a horizontal position, rotating the antennas to restore copolarization, and recording data. Offline processing is used to calculate power offsets per transmitter and frequency, therefore minimizing deviations from the normalized mean for the four receivers. If the receivers are at the same height, the normalization process gives offset corrections for each receiver. If the receivers are not at the same height, the normalization does not yield receiver offsets, but is still used to give each receiver an equal vote in determining transmitter offsets. (The normalization should really be by signal-to-noise ratio rather than equal vote.) This process includes the antennas within the calibration procedure. Without it, the factory measurements of antenna gain are used in computing propagation loss.

All calibration data are archived for offline processing use. Recorded data generally include the then-current calibration data in each collection file. In addition, diagnostic signals including YIG temperature-per-receiver and signal analog-to-digital (A/D) saturation counts are recorded.

### Display Modes

Three display options are available for one-way propagation factor. All three have selectable scaling. The three options are x-y line plot, which overlays data for the collection interval; a static plot, which color-codes propagation factor versus frequency and height and refreshes for each loop; and a dynamic display of color-coded propagation factor versus time, which overwrites after a selected data length. In all three cases a single display panel or four display panels may be chosen. Whereas considerable flexibility exists in display options, a new option may not be selected without paying up to 2 min of dead time for communication and setup.

Frequency-Line. In the x-y, or "frequency-line" plots, up to 16 color-coded lines may be displayed per panel. With the 4 panels, the full set of 16 frequency profiles may be observed for the 4 receivers. Since this display overwrites, it becomes hard to read when propagation is fluctuating.

Complete freedom exists to allocate frequencies and receivers to a panel, with a limitation of 16 lines per panel. These options are particularly useful in offline processing. In Section 4 of this document (pages 4-2 through 4-9) examples are shown where several profiles are overwritten for each frequency.

Static. The "static" plot has generally been the preferred one for online observation. No history is preserved, but the current values are clearly discernable. A panel covers the 10 heights and 16 frequencies for a receiver. The four-receiver display is easily read and assimilated. An example of a static plot is on page 4-12 of Section 4.

Dynamic. The "dynamic" plot is useful for offline processing but has been little used online. The horizontal axis of the dynamic plot is time, and the vertical axis is transmitter height. One or four panels are displayable to show the pathloss as detected by one or all four of the receivers. Color is used to represent loss levels. A typical plot is shown on page 4-20 of Section 4.

FFT-Line. For diagnostic purposes, the FFT plots may be displayed. Considerable flexibility exists in the receivers and frequencies that may be displayed, including the display of all at one time, but the display is limited to a single panel and is overwritten. In this mode, processing time puts a limitation on the combination of spectral width displayed and frequency switching rate. This plot does not work in the offline mode.

### Offline Playback Unit

The receiver site has a separate computer, display, tape unit and Bernoulli unit for offline processing. In this way an overnight collection tape may be removed and copied to Bernoulli for fast processing, with little interruption of ongoing data collection. The receiver system may also be used for offline processing from taped signals, but this interrupts data collection. In offline or online modes, propagation factor may be displayed relative to any reference condition for which a file has been computed (using a propagation model) and entered. In general, propagation factor relative to free space is displayed.

### Performance

The one-way free space propagation loss at a wavelength,  $L$  meters, between the antenna ports of an aligned pair of antennas with gain,  $G$ , at a range of  $R$  meters in free space is given by:

$$\text{loss} = \left( \frac{GL}{4\pi R} \right)^2$$

The antenna gain is 11.7 dB at 2 GHz and 13.5 dB at 18 GHz. The loss at 10 nmi range is then 100.4 dB at the lower band edge and 115.9 dB at the upper. For a nominal 20-dBm transmitted power, the free space signal-to-noise ratio is then computed using the values in Table 2-1.



TABLE 2-1. MPMS PERFORMANCE, SIGNAL-TO-NOISE RATIO

	Frequency	
	2 GHz	18 GHz
Transmitted power, dBm	+20.0	+20.0
Propagation loss, dB	-100.4	-115.9
Received signal, dBm	-80.4	-95.5
*KT, dBm/Hz	-174.0	-174.0
Noise Figure, dB (includes YIG and audio filter)	10.0	10.0
Bandwidth, dBHz (25-kHz sampling rate)	43.9	43.9
Integration Gain, dB (4096 points I&Q)	-36.0	-36.0
Weighting loss (Hanning)	1.0	1.0
Mean noise, dBm	-155.1	-155.1
<b>Signal to mean noise ratio, dB</b>	74.6	59.6
Using Only Real Signal Component (-3 dB)	71.6	56.6
Using Only Real Signal Component and 512 points (Integration Gain down by 9 dB)	62.6	47.6

\* Boltzmann's constant (K)  $\times$  temperature (T), 290 K

In the case of shorter transforms, a number of transforms are averaged so that, even though the mean noise is not reduced, the noise fluctuations are reduced allowing operation closer to the mean. The performance margin was good enough that the additional step of computing signal power from measured noise and measured signal plus noise was not taken.

## ACCURACY

The overall accuracy of the system is dependent heavily on receive and transmit calibrations, gain uniformity between antennas, and the YIG filter calibration with temperature, antenna alignment, and antenna pattern. Measurements of these parameters were made throughout testing, but were often precluded by adverse weather conditions. The following sections examine each of these parameters, which contribute to system accuracy.

Receive Calibration Accuracy

In this section, Receiver 1 gain calibration measurements are compared using two calibrations that were performed about 1 month apart. Both calibrations were performed at all 16 frequencies. The first column of numbers shown in Table 2-2 lists the frequencies used during calibration and data collection, and the second column lists the dB differences between the gains measured by the two calibrations.

The mean delta value between the two Receiver 1 calibrations is then -1.64 dB, and the standard deviation is 0.88 dB. These values indicate that the receiver gains 1) did not drift significantly with time; 2) did not affect the overall system accuracy more than 2.93 dB, which is the largest excursion shown in the values in Table 2-2; and 3) on the average, degraded the overall system accuracy only 1.64 dB.

TABLE 2-2. RECEIVER 1 CALIBRATION DATA

Frequency (GHz)	Delta (dB)*
2.365	-1.14
3.600	-1.60
4.635	-0.46
5.900	-1.73
7.145	-1.94
7.530	0.28
8.475	-0.99
9.295	-0.78
10.400	-1.85
12.300	-2.93
13.390	-2.85
13.570	-2.26
14.490	-2.36
15.000	-1.09
15.900	-1.55
17.350	-2.92

\* Difference in two gain calibrations, 1 month apart, at each frequency.

### Transmit Calibration Accuracy

Two calibrations of Transmitter 8 are compared in this section. This transmitter was chosen because it was calibrated on two separate occasions approximately 1 month apart while at Wallops Island. (A full calibration of all the transmitters was conducted twice during this period at Wallops Island, but calibrations were conducted within a week of each other, which was not time enough to observe accumulated drift. The calibrations prior to these were made months earlier while the system was still at Dahlgren undergoing acceptance testing. As a spot check while the system was at Wallops Island, only Transmitter 8 was calibrated with a suitable time interval for this analysis. Adverse weather and the remote location of the transmitters on Parramore Island prevented more calibrations there.) As stated earlier in Section 2, the transmitters are calibrated by comparing the system's internal power-monitor values to the power-meter readings collected at the input to the transmit antennas. The two calibrations of Transmitter 8 showed a mean difference of only  $-0.157$  dB between the power-meter readings taken approximately 1 month apart. The differences between the power-monitor reading just before the second calibration and the calibration power-meter readings are listed in Table 2-3 to give a feel for the amount of change induced by the calibration. Since 2 different sets of frequencies were used for the 2 calibrations, only 13 frequencies were in common; these values are listed in the left column. The maximum excursion for these 13 frequencies was less than 1 dB, and the mean change was  $-0.37$  dB.

TABLE 2-3. TRANSMITTER 8 CALIBRATION DATA

Frequency (GHz)	Calibration/Monitor delta* (dB)
2.365	-0.780
4.635	0.202
7.145	-0.107
7.530	-0.180
8.475	-0.476
9.295	-0.799
10.400	-0.179
12.300	-0.328
13.390	-0.441
13.570	-0.788
14.490	0.229
15.000	-0.998
17.350	-0.201

\* Difference between power-meter readings and power-monitor reading before second of two calibrations, 1 month apart.

### Receive Channel Comparison

During acceptance testing at Dahlgren, a test was performed to measure the differences in the four receive channel responses to identical inputs. Three frequencies were chosen for this test, 2.365, 10.4, and 17.35 GHz, to include the extremes and midpoint of the frequency range of the system. First, Receive Channels 1 and 2 were fed signals from Receive Antenna 2, where the output had been split. Next Receive Channels 3 and 4 were fed signals from Receive Antenna 3. In the graphical output that was saved, the difference in the response of Receive Channels 1 and 2 and Channels 3 and 4 was 1.5 dB at the worst, and in some portions of the graphical output, no difference was discernable. The remaining receive-channel to receive-channel differences would then be caused by the YIG filters used as prefilters on each receiver. Since the YIG filters are temperature- and frequency-dependent in terms of their passband, these filters were characterized across frequency in the factory and temperature-compensated using a thermistor to measure temperature as the YIG filter was tuned. Unfortunately, a full range of temperatures was not used during the factory tests, and during the winter at Wallops Island, the necessity for further YIG filter calibration at lower temperatures was evident.

### YIG Filter Calibration

As stated in the previous section, a major contributor to receive channel-to-channel discrepancies was the use of YIG filters on each receiver. These discrepancies were worse for some frequencies and receivers than for others. Because of the multiplicity of frequencies (some closely spaced) and receivers, these problems were actually evident to the eye, allowing field detection and correction of the problems. For the most part, the data can be screened for bad values at a given frequency in those situations where the YIG filters were not calibrated at the operating temperature of the receivers at the time of data collection. An automated YIG filter calibration scheme was devised and used during tests whenever temperature changes warranted. When the YIG filters are obviously mistuned, values have been observed to deviate as much as 12 dB, which is easily detectable. When the YIG filters are properly tuned, only the passband ripple of the filter affects the variability in the output level. The passband of each of the YIG filters has been measured across the 2 to 18 GHz band with the average passband error for all frequencies and all four receivers being 1.1 dB. The worst passband ripple value for all receivers was approximately 1.3 dB.

### Antenna Gain Accuracy

As stated earlier, the antennas were not part of calibration except as included with system calibration. Also as stated earlier, the antenna gains were measured in detail for two of the antennas and only spot-checked for the rest. This was thought to be adequate because the antennas were made using precise machinery such that each antenna should be identical to the next within milling tolerances. Verification of antenna gain was attempted in the field near the close of the tests, along with accuracy measurements of the antenna pointing angle.

The antenna gain was checked in the field by the following process: The receiver calibration hardware was set up to inject the receive calibration signal directly into the lowest receiver (at the antenna terminal). Then the observed system output was set to a desired level using the precision

attenuator of the calibration hardware, and this value of attenuation and signal strength was recorded. Next the same signal was fed to the antenna-under-test, which was aligned in front of the lowest receiver a distance of 26.7 ft away. The signal level was adjusted to be equal to that in the previous step by varying a precision attenuator, and this value of attenuation was recorded. This process was repeated for distances of 7 and 14 ft as well. The difference in space loss was calculated and compared with the difference in the attenuator settings for the different ranges.

The antenna gain measurements were made at four frequencies, 5.9, 10.4, 13.95, and 17.35 GHz, and for three antennas, one of which was known to be bad. Results supported that the gain was down in the antenna that was known to be bad. Results for the other two antennas showed that the two tracked each other well (deltas were less than 1 dB), but gain-versus-frequency results were mixed. At 5.9 GHz, agreement between calculated and measured loss was good or within about 1.2 dB, meaning antenna gain values were within 0.6 dB of factory-measured values and probably at the limit of measurement accuracy. At 10.4 GHz, agreement between measured and calculated loss was worse, varying from 2.95 to 3.88 dB, which could be interpreted as an antenna gain 1.7 dB above the factory-measured value. At 13.95 GHz, agreement was as good as or better than at 5.9 GHz. At 17.35 GHz, agreement was quite poor, varying from 4.99 in the positive direction to 9.37 in the negative direction, indicating a change in gain from a 2.5-dB increase to a 4.7-dB decrease. Since these measurements were made in the field in a short amount of time, some concerns remain as to multipath effects, near-field/far-field distance, and other measurement errors. Also, since only a few frequencies were measured, not the comprehensive set used during data collection, no adjustment reflecting these measurements has been made to the antenna gain tables.

An examination in detail of the antenna gain tables and measured antenna patterns showed that for certain higher frequencies, the antenna patterns were not level, actually dipping near the center or boresight. Therefore, an offset was applied to the affected boresight gain values to account for the dip in the measured antenna patterns. After the offset was applied, the measured propagation loss values were decreased for those frequencies that exhibited the boresight dip in gain. The adjustments in the boresight antenna gain were significant, that is, greater than 0.5 dB, only at the following frequencies: 12.3, 13.39, 14.49, and 15.0 GHz (see Table 2-4). The largest change in boresight antenna gain was 2.45 dB at 12.3 GHz. A large increase in loss or decrease in propagation factor was noticed in much of the data between 10.4 and 12.3 GHz before the boresight gain correction; and with this change in the boresight antenna gain, the transition in loss from frequency to frequency is smoother, with the gross trends remaining the same.

The antennas used in the above discussions are to be remeasured in a laboratory environment to obtain current detailed antenna patterns. These patterns will be compared with those provided by the manufacturer when the antennas were purchased, and any necessary amendments to the above statements will follow in a separate report. New antennas will be used in future data collection efforts, especially if the transmitter array is placed onboard a boat. The beamwidth necessary for that experiment will probably force an overall lower gain, but since the system signal margin is good, a moderate reduction in gain is not considered a problem.

As a final step in the field check of antenna gain, the alignment of the transmit and receive antennas was verified by rotating the receive tower in its vertical position so that the receivers as a set were changed in azimuth pointing angle. The received power was monitored during this process with the results showing that the antennas were aligned correctly in their original position.

TABLE 2-4. ANTENNA GAIN

Frequency (GHz)	Original Gain (dB)	True Boresight Gain (dB)
2.365	12.07	N/C
3.600	10.95	N/C
4.635	11.10	N/C
5.900	11.13	N/C
7.145	10.85	N/C
7.530	11.20	N/C
8.475	11.45	N/C
9.295	12.07	N/C
10.400	12.48	N/C
12.300	13.52	11.07
13.390	13.63	12.05
13.570	13.15	12.77
14.490	12.95	12.27
15.000	12.95	11.75
15.900	13.23	12.98
17.350	14.38	N/C

\* N/C = No Change

### Accuracy Summary

Given the individual contributors just discussed, the overall system accuracy is on the order of 2.6 dB for all the factors given in the previous sections except for gross YIG filter mistuning (see Table 2-5). Recorded data can be screened for hardware problems fairly easily because of the inherent module redundancy for transmitters and receivers and because the number of frequencies used allows some frequencies to be closely spaced and still cover the 2 to 18 GHz band. In other words, while the complexity of the system in some ways added to the difficulty of calibration, it also provided checks for bad data that could be seen during data collection. There are areas of uncertainty in all of these measurements that hopefully will improve as the system is used more, as new procedures are developed, and as hardware improvements are made. However, the propagation changes and major features noted in the data are clearly all of such significant magnitude that the system errors in accuracy are small compared to the overall measurements of interest. Propagation changes and major features noted in the data are discussed in Section 4, "TESTS RESULTS."

TABLE 2-5. SYSTEM ACCURACY

Component	Average Accuracy Values	Worst Excursions
Receiver Calibration	1.64 dB	2.93 dB
Transmitter Calibration	0.37 dB	0.998 dB
Antenna Gain	1.0 dB*	2.45 dB**
YIG Passband	1.1 dB	1.3 dB
Normalized RMS Error	2.60 dB†	

\* This value was arrived upon using antenna gain measurements made in the field considering the entire frequency range.

\*\* This value was taken from the boresight corrections.

† The antenna gain error applies twice (once for transmit and once for receive) in the computation of the system's mean error.



### SECTION 3

#### METEOROLOGICAL DATA COLLECTED

The propagation measurements were made as part of a larger test function at Wallops Island. Meteorological data were collected in support of the overall test effort and can be used as needed to help interpret measured propagation loss and to compare modeled versus measured pathloss.

##### METEOROLOGIC (MET) VAN

A van, located near building Z41 during the tests, collected local meteorological data and served as a base collection site for several remote sensors, including a wave rider buoy and a tide gauge. Temperature and relative humidity were collected at heights of 3 and 21 ft above ground. Wind speed and direction, pressure, and rain rate were also collected. All values were collected at least as often as every 30 min, and the rain rate was collected on a 1-min interval. The wave rider buoy collected meteorological data that included air temperature, water temperature, relative humidity, wind speed and wind direction, as well as wave height and statistics. The water temperature sensor was damaged early in the test period and the relative humidity sensor proved unreliable during the latter part of the test period. The tide gauge was located near Parramore Island and recorded average water level and water temperature several feet below the surface. The buoy meteorological data and the tide data were collected first on a 10-min interval, but that was later changed to a 30-min interval to avoid data storage overflow problems during periods when data telemetry was not working.

##### 100-FT METEOROLOGICAL POLE (10-SENSOR ARRAY)

Meteorological data were collected using an array of 10 sensors mounted on a 100-ft tower (the same tower used to support the RF propagation measurement receivers). Nine of the sensors were mounted at fixed heights and the tenth was mounted on a moving shuttle which travelled between the fixed sensors, acting as an offset and calibration measurement. The primary output of this sensor array is refractive profiles every 5 sec, which could then be time-averaged as desired. The tower's location was somewhat more inland than desirable for measurements of this kind to avoid moving the entire setup in the event of severe weather. The following data were collected whenever possible (depending on high winds and relative-humidity sensor saturation) to calculate refractivity profiles:

- Time [Universal time coordinated (UTC)]
- Temperature [Celsius (C)]
- Relative Humidity (percent)
- Position of the moving sensor

Atmospheric pressure as a function of height is derived from the pressure measured at the MET VAN and the standard relationship between pressure and height. This array of sensors was previously tested, and the data it collects were described in an article in the Naval Surface Warfare Center, Dahlgren Division (NSWCDD) *Technical Digest*, September 1992 issue.<sup>1</sup>

#### 100-FT METEOROLOGICAL TOWER (SINGLE SENSOR), Y85

Another 100-ft tower was used to measure refractive profiles further inland using a single moving sensor package. This tower was supported by a large permanent tower, known as Y85, located on Wallops Island. Profiles of temperature and relative humidity were used to make refractive profiles versus height as the sensor package moved up and down the tower. These profiles were made approximately every 11 min with each profile consisting of approximately 50 points, allowing for a data point every 2 ft. Often this measurement system suffered from relative-humidity sensor saturation as well as mechanical problems primarily caused by high winds; therefore, data from this tower are not all-inclusive for the test period. The following data were recorded:

- Time (UTC)
- Temperature (C)
- Relative Humidity (percent)
- Sensor Height (m)

#### APPLIED PHYSICS LABORATORY (APL) METEOROLOGICAL SUPPORT

APL was also involved with the collection of meteorological data using several sensor systems: the meteorological SLED and other meteorological sensors mounted on their research boat, *Chessie*, and meteorological sensors mounted on a helicopter. Most of the data from these sources are used to calculate refractive profiles. The data collected from *Chessie* included the following:

- Time (UTC)
- Air temperature (C) at 0.02, 1.0, 6.0, and 10.0 m
- Relative humidity at 0.02, 1.0, 6.0, and 10.0 m
- Pressure (mb) at 0.02, 1.0, 6.0, and 10.0 m
- Sea surface temperature (C)
- GPS latitude and longitude versus time

The helicopter flew a sawtooth pattern between 10 and 1500 ft in altitude. Altitude data were collected by a dual-antenna radar altimeter. All helicopter data were recorded at a 2-Hz rate. The data collected by the meteorological helicopter included the following:

- Air temperature (C)
- Pressure (mb)
- Relative humidity
- Altitude (ft)

On certain test days when the *Chessie* was used but the helicopter was not, upper air soundings (up to 1000 ft) of temperature, pressure, and relative humidity were collected using an aerostat. However, the upper air soundings were not possible on many occasions because of high winds.

#### NASA GROUND STATION METEOROLOGICAL DATA

Data were also collected at the standard NASA meteorological sensor locations and provided on floppy disk. The following data were collected:

- Time (UTC)
- Wind direction (deg)
- Wind speed (mph)
- Maximum wind speed (mph)
- Temperature (F)
- Dew point (F)
- Pressure (in.)
- Rain (in.)

#### IR RADIATION METEOROLOGICAL BUOY

A buoy was anchored along the line of sight between building Z41 at Wallops Island and the equipment at Parramore Island. This buoy's function was to collect meteorological data necessary to assess the refractive environment for IR. The data collected by the buoy were used as part of an IR propagation measurement setup to collect data side by side and simultaneously with the RF propagation measurements. Results from the IR propagation measurements and the joint analysis of the IR and RF propagation measurements are discussed in separate reports. The buoy was equipped with an array of eight temperature probes spaced between the sea surface and a height of 118 in. Shortly after the buoy's deployment, an equipment failure led to very little data being collected during the test period.

## SECTION 4

### TEST RESULTS

This section outlines data collected specifically during the week of 21 to 25 March 1994. This week was picked because it encompassed data variations generally seen throughout the experiment and also provided a manageable data set for this report. The entire body of data is being screened as well, and will be discussed in follow-on reports if significant features are evident.

There were several types of temporal variation observed in the data that were collected, including 1) gradual fades from strong ducting to severe subrefraction, 2) rapid fluctuation characterized by null shifts in height-versus-loss profiles during periods of generally low loss or ducting as well as during periods of high loss or subrefraction, and 3) rapid fluctuation in a smoother, orderly fashion showing a twisting and "fanning" of profiles. Most of these temporal variations are more easily seen through video playback of the data, but for this report a series of graphs will be used to show the relative changes. Start and stop times are noted at the bottom of each graph. Data are presented in several display modes, which were discussed in Section 2. The graphs of these display modes are explained as necessary.

#### TRANSITION FROM DUCTING TO SUBREFRACTION

In the "frequency-line" plots, Figures 4-1 through 4-5, transmitter height is indicated along the vertical axis of each of four graphic squares, and one-way pathloss (in dB) relative to free space (or one-way propagation factor) is indicated along the horizontal axis. The color codes on the right, one for each graph from left to right, top to bottom, are used to distinguish between frequencies per each receiver: the first number indicates which receiver output is graphed and the second number indicates which of the 16 frequencies is graphed; e.g., 2,11 means Receiver 2, Frequency 11. The key to the number and/or height of transmitters, receivers, and frequencies is to the left of the figure.

Figures 4-1 through 4-5 show the transition between ducting and subrefraction that occurred on 24 March 1994 from about 00:30 to 03:10 local time.

In Figure 4-1, strong null structure can be seen caused by the duct supporting multiple modes at the higher frequencies. Receiver 2 does not show the null structures versus height for the region measured, but does show better overall uniformity of performance with height (irrespective of frequency) than the other receiver heights. Individual profile shapes have less uncertainty than the absolute propagation value. The shape is affected only by the transmitter power errors and the transmitter antenna gain differences. Rapid changes in the shape are more reliable yet, since neither of the error sources show other than very slow changes. Since these plots overlay with time, lines

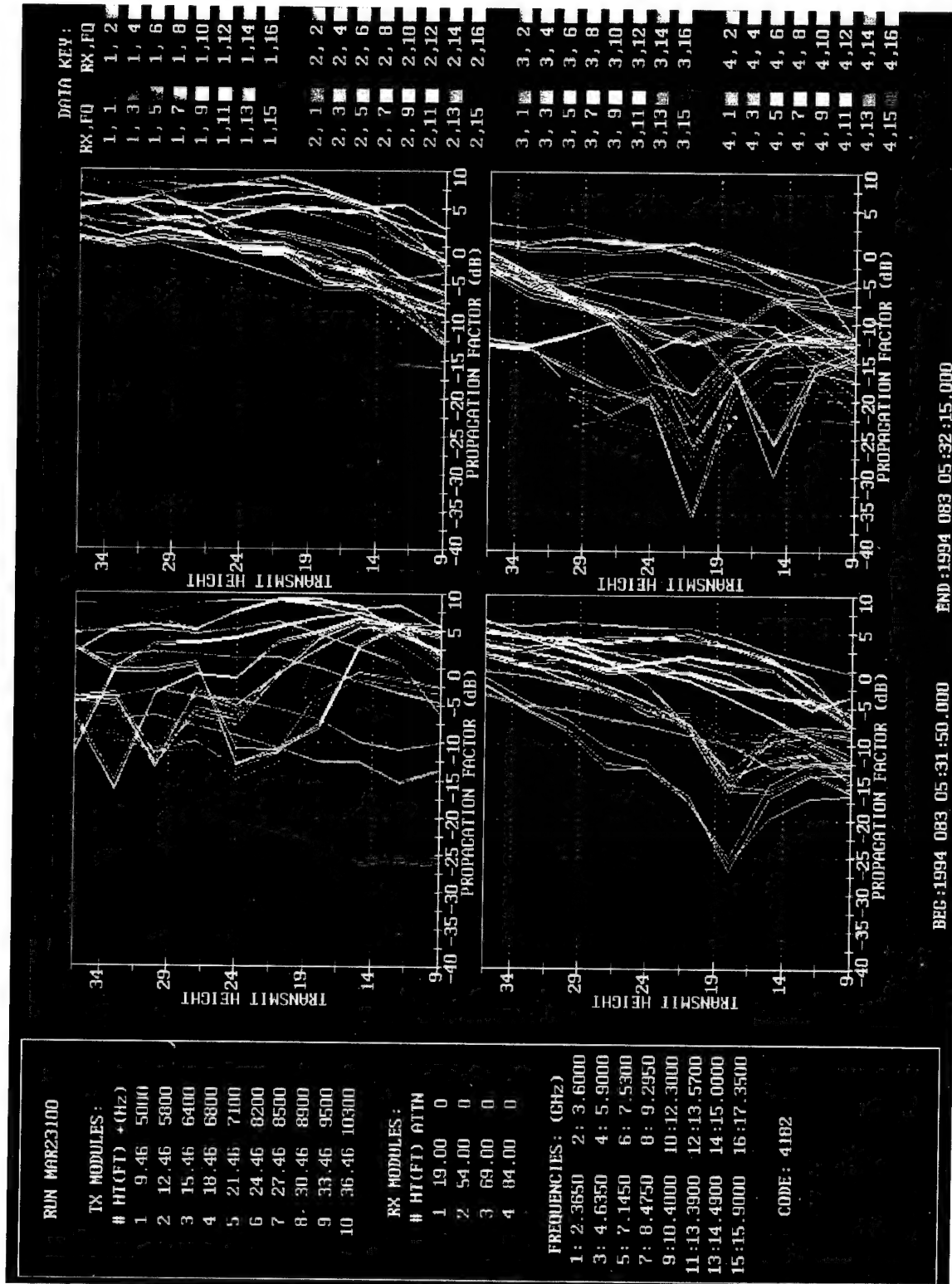


FIGURE 4-1. FREQUENCY LINE PLOT 24 MAR 94 05:31 UTC

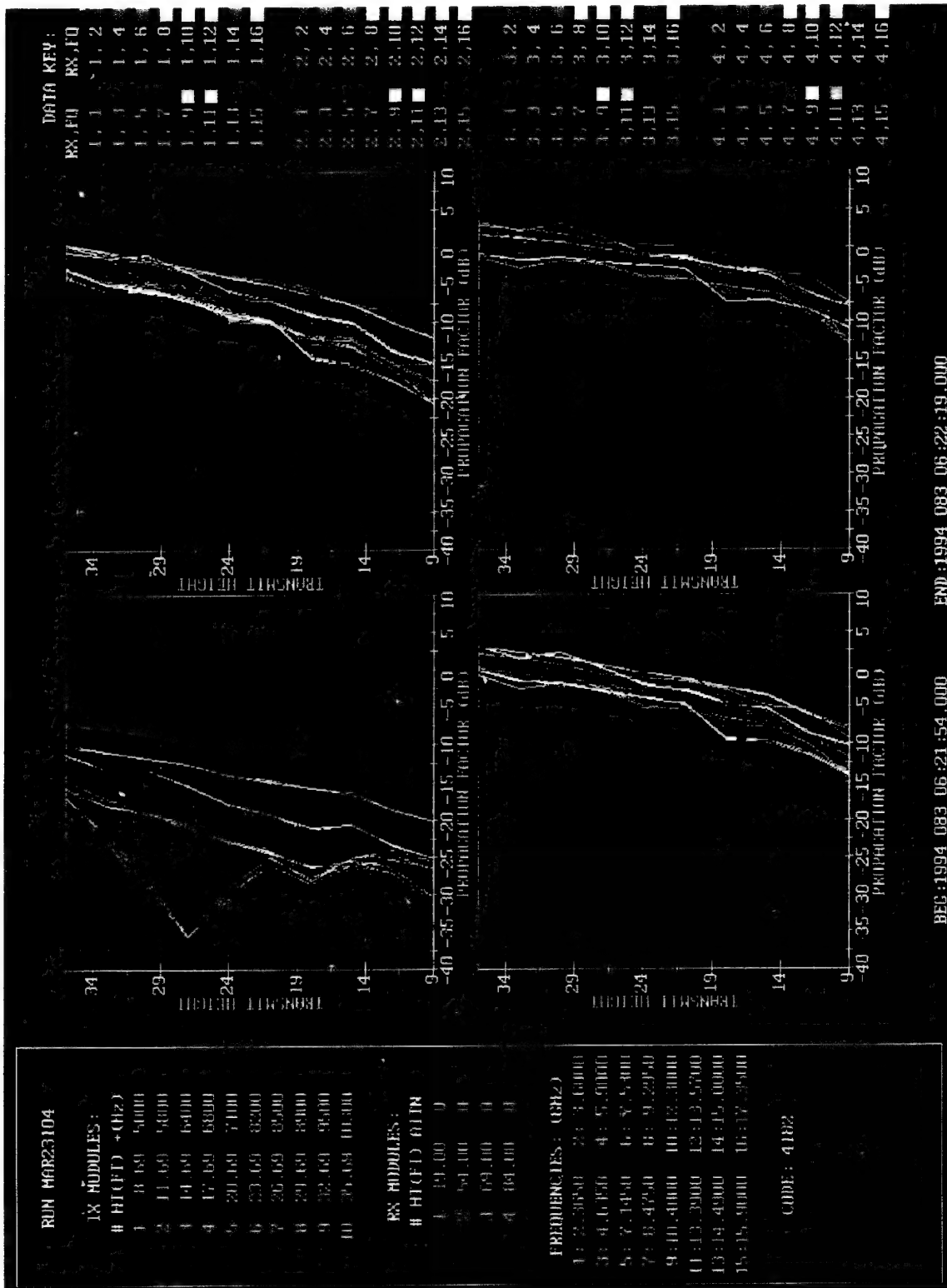


FIGURE 4-2. FREQUENCY LINE PLOT 24 MAR 94 06:21 UTC

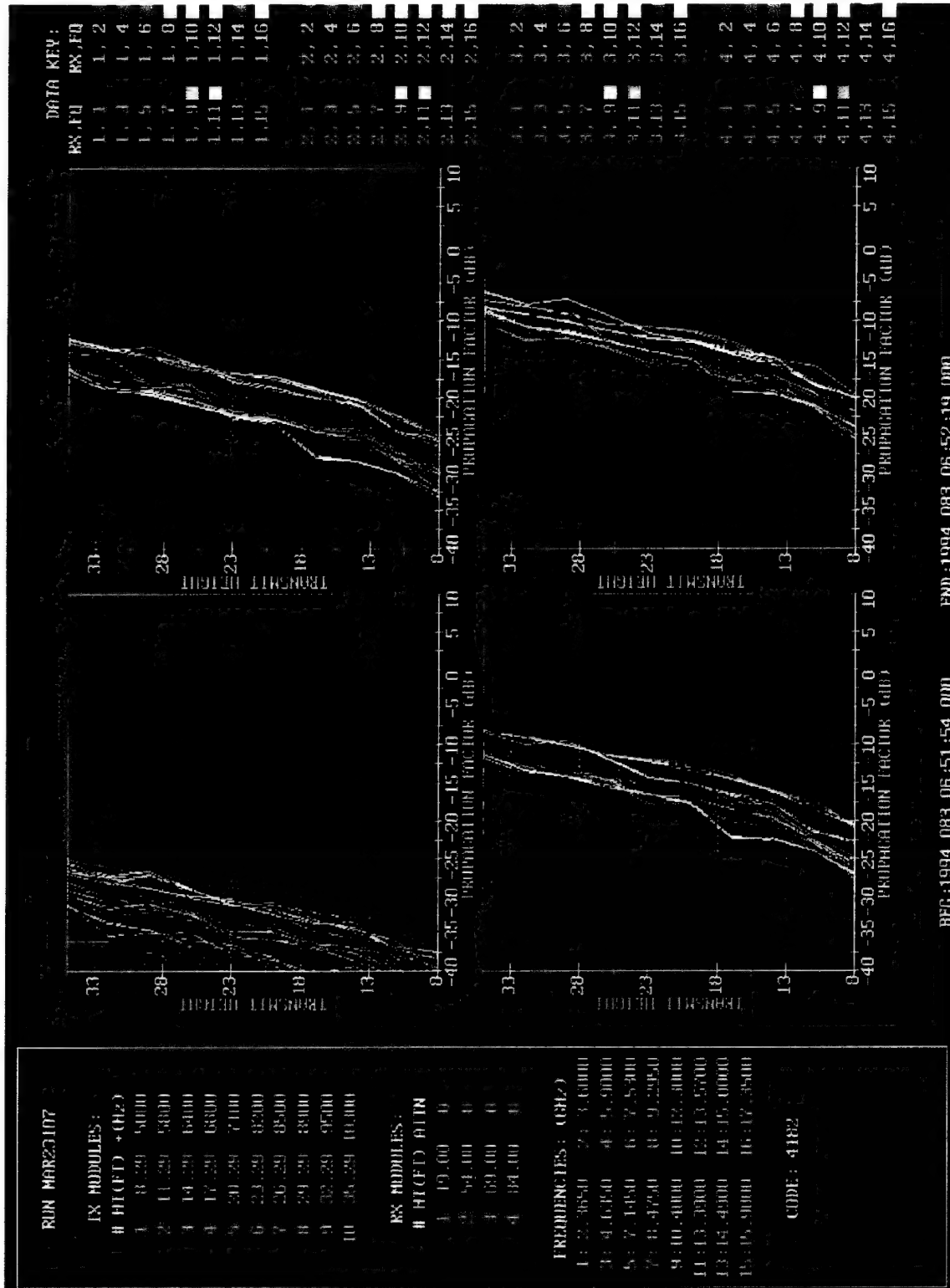


FIGURE 4-3. FREQUENCY LINE PLOT 24 MAR 94 06:51 UTC



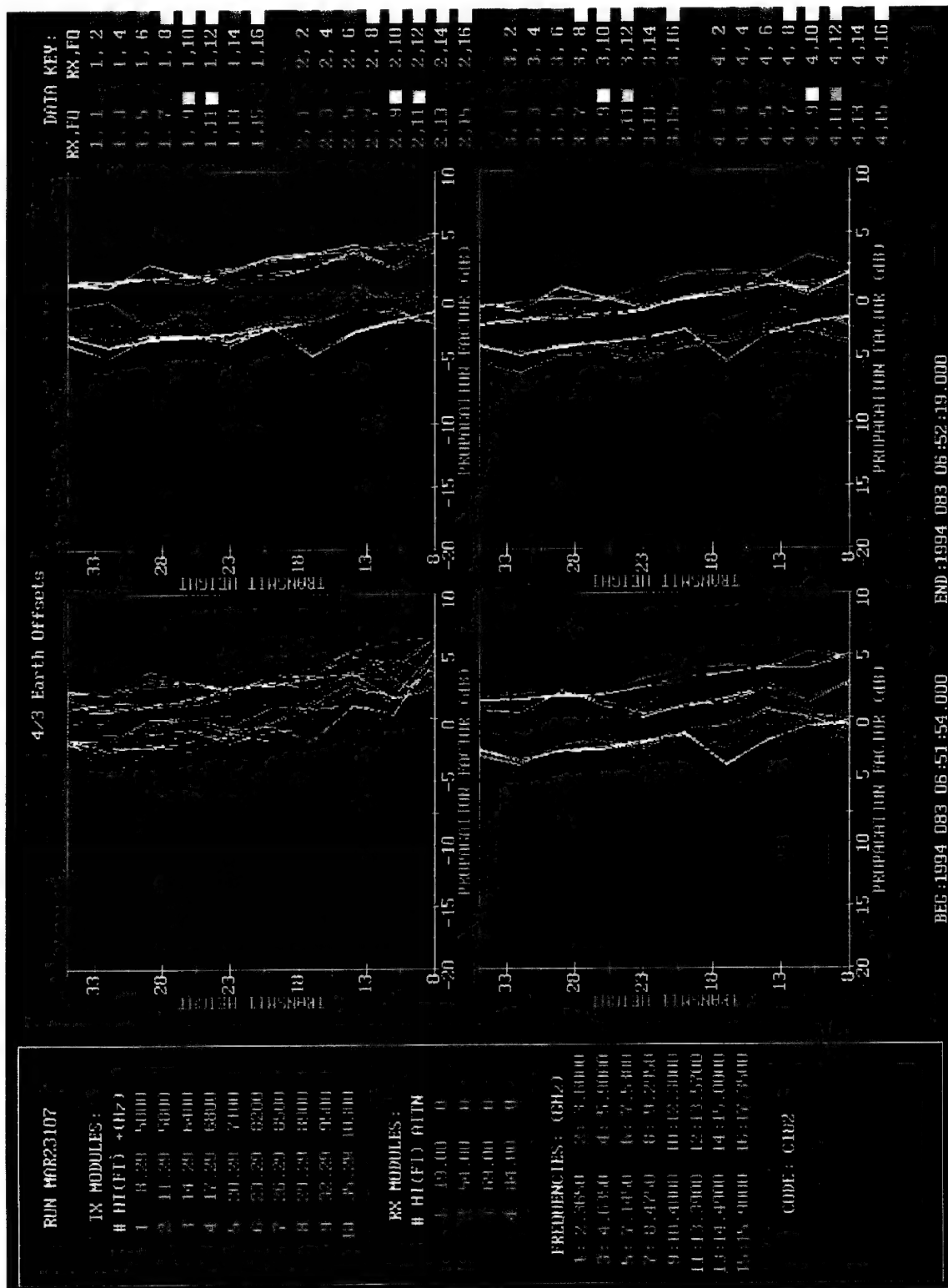


FIGURE 4-4. FREQUENCY LINE PLOT 24 MAR 94 06:51 UTC, 4/3 EARTH REFERENCE

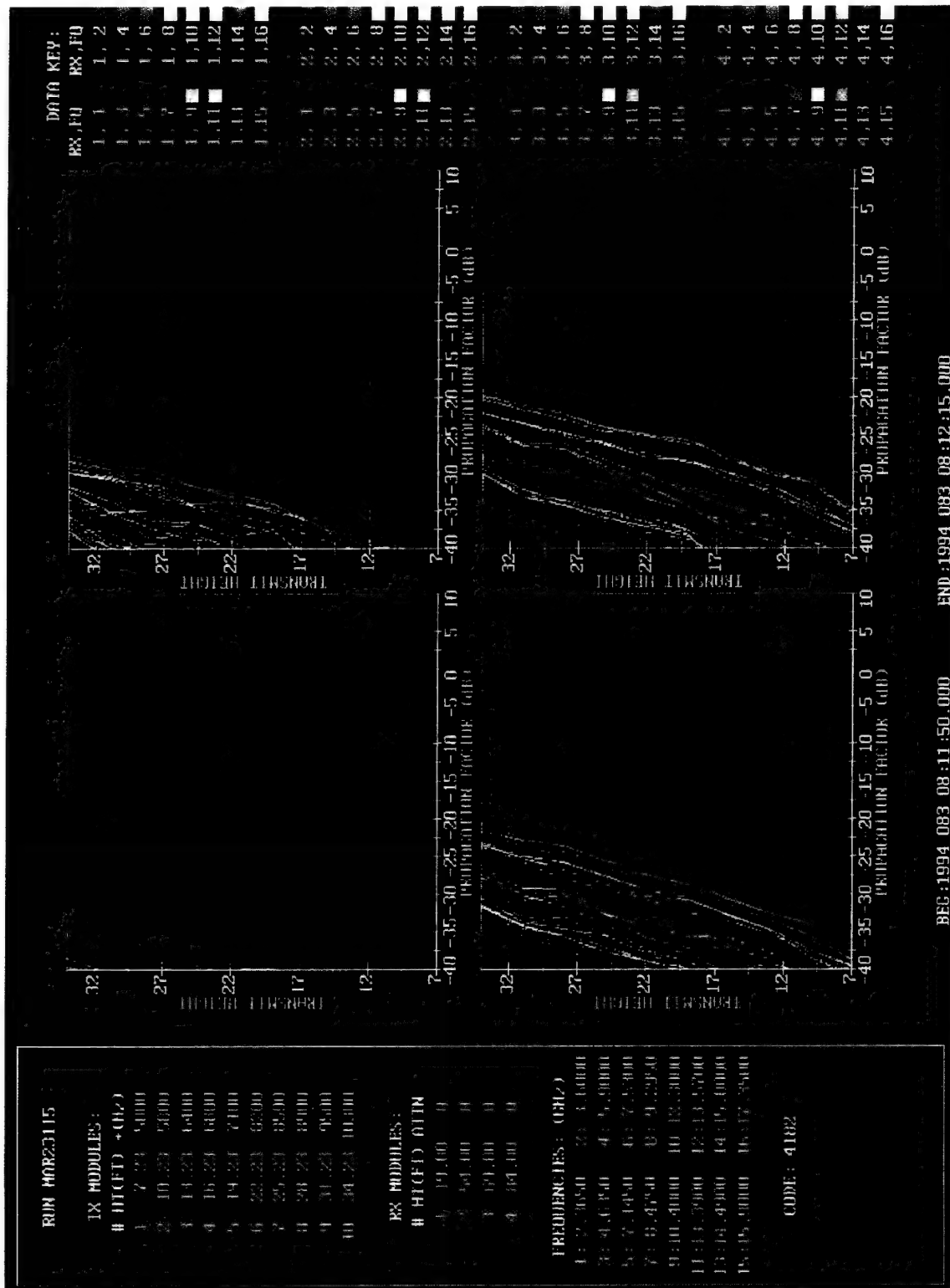


FIGURE 4-5. FREQUENCY LINE PLOT 24 MAR 94 08:11 UTC

with the same color indicate the fine-scale time variation with a new line being plotted every 8 sec. For these data, the placement of the null in height did not vary quickly with time, but the depth of the null did. Loss was low during the beginning of this period, with some values as much as +7 or +8 dB above free space one-way at the 7.145-GHz frequency on Receivers 1 and 2. Figure 4-2 shows the beginning of the change from ducting to subrefraction. As this change took place, the null structures disappeared, with Receiver 1 showing these structures longest at higher frequency.

In Figure 4-3, a transition through 4/3 earth or standard-atmosphere loss values took place. Figure 4-4 shows the same data referenced to the one-way pathloss as calculated for 4/3 earth or standard atmosphere. The measured pathloss profiles are in general grouped around 0 dB relative to 4/3 earth and are nearly vertical, indicating that refractive conditions were likely close to that associated with 4/3 earth. However, there are differences in loss relative to 4/3 earth for all four receivers, and these differences appear somewhat frequency-dependent. The lowest frequencies on Receiver 1 have the greatest absolute difference of 15 dB less than the values calculated for 4/3 earth. The frequency ordering shown is variable from receiver-height to receiver-height. Receiver 1 showed the least loss for Frequency 6 (7.53 GHz) with lowest loss values clumping around Frequencies 4 through 10 and Frequencies 14 and 15; Receiver 2 showed least loss for Frequencies 5, 6, 8, 9, and 10 and a second-best cluster around Frequencies 11 through 16; Receiver 3 showed least loss for Frequencies 8, 9, and 10, and a second-best grouping including Frequencies 4 through 7 and 11 through 16; Receiver 4 showed least loss for Frequencies 5 through 10 and second-best grouping for Frequencies 11 through 16. Taking all four receivers into account, Frequencies 5 through 10 (7 to 12 GHz) performed the best; Frequencies 4 and 11 through 16 (5.9 and 13.3 to 17.3 GHz) performed nearly as well; and Frequencies 1 through 3 (2.4 to 4.6 GHz) performed the worst. This frequency ordering is not exactly as predicted for standard atmosphere, which predicts the least loss for the highest frequency; however, there is no assurance that the environmental profile was exactly 4/3 earth at the time the data were collected.

By the time the data in Figure 4-5 were taken (about 1 hr and 20 min later than Figure 4-4 data), values of loss are subrefractive and are off-scale almost entirely for Receiver 1. The highest receiver shows the least loss of the four with no frequency showing less loss than 20 dB relative to free-space loss. However, the frequency ordering for these higher loss environments is not as expected, with some of the lower frequencies showing less loss than the higher frequencies. As with the earlier discussion, frequencies in the 5.9 to 9.3 GHz range seemed to suffer the least amount of loss, with 7 to 7.5 GHz consistently showing the least amount of loss. The highest and lowest frequencies (2.4 to 4.6 and 13.3 to 17.3 GHz) suffered the most loss in general with their curves lying on top of each other in many cases. Overall, a clear preference for the midband of frequencies is evident in these plots from about 7.145 to 10.4 GHz, which show lower overall loss values and greater uniformity of loss versus height during the ducting period.

For a number of years, APL has been operating a C-band link to detect propagation fades like this one along nearly the same path.<sup>2</sup> The character of the data from this link was compared with the data collected by MPMS for the timing of the fade transition, and good agreement was noted. Unfortunately, no local (Patuxent River) weather radar data were available during this period, and no helicopter or boat meteorological data were available because of the time of day this transition occurred. However, the MET VAN data showed that the wind speed increased 2 kn, the temperature dropped on the order of 4 C, and humidity was generally on the rise.

There were two transitions like the one analyzed above, during the week covered by this report. During the beginning of the week, propagation was in general poor (standard atmosphere or worse) until a ducting period occurred on 22 March 1994 at 15:22 UTC. This period of strong propagation lasted approximately 38 hr, during which one short fade period appeared at 07:50 UTC 23 March 1994 and lasted only about 20 min. A period of very poor propagation began about 05:30 UTC 24 March 1994 and lasted over 32 hr; the system was turned off because of an impending power outage on 25 March 1994.

## RECEIVER HEIGHT EFFECTS DURING DUCTING

Figures 4-6 and 4-7 are "static" plots showing four graphic squares, each made up of 160 smaller rectangles color-coded as shown to represent one-way pathloss relative to free space (in dB). White indicates those values off-scale in a positive direction (less loss), and black indicates those values off-scale in a negative direction (more loss). The four graphic squares represent the four receivers at heights of 19, 54, 69, and 84 ft above mean sea level. The 10 transmitters and transmitter heights are given by each of the smaller squares vertically from lowest to highest (Transmitter 1 was 7.7 ft above mean sea level; changes in tide height account for any differences from this value). The table of values in the upper left corner of the graph gives the transmitter number, its height above water in feet and the offset frequency used in spectral analysis to separate each of the transmitters. When the tide value is known, the transmitter heights can be offset by this amount to give the actual transmitter height above water at the time the data were collected; this is an offline processing feature. Frequency is covered by the 16 numbered steps listed in the lower left corner and by the smaller squares along the horizontal axis in each of the four graphic squares, with the frequencies increasing from left to right.

The static plots in Figures 4-6 and 4-7 are for 22 March 1994 at approximately 14:39 UTC and for 23 March 1994 at approximately 13:53 UTC. This display refreshes every 8 sec, so the data shown in Figures 4-6 and 4-7 are for one snapshot of an 8 sec interval. The propagation factor values indicate that propagation is better than standard atmosphere, or that a duct was present in both cases; however, the rank ordering versus receiver height is reversed from one plot to the next. This ordering is clearly evident if one notices the number of white spaces (values better than 0 dB relative to free space) for each receiver on the two figures. The meteorological data from helicopter soundings that were collected nearest in time to the MPMS data (and merged with evaporation-duct height information) were used to compare propagation model output to the measured pathloss values. Refractive profiles were then input to the RF propagation model, PCPEM.<sup>3</sup> Although PCPEM will accept range-varying refractive profile input, only the first in the range-varying set of profiles from the helicopter was used because the path to Parramore, along which the MPMS data were collected, was completely coastal, and the helicopter was flying a radially outbound path from Wallops Island on 135 deg true. The refractive profile collected by the helicopter when it was nearest to shore was thought to be more representative of the MPMS data path than the entire helicopter run.

Figure 4-8 shows the propagation model output for Frequency 6, or 7.53 GHz, for the refractive data collected during the time period covered in Figure 4-7 (the sixth column of data for each of the four receivers in Figure 4-7 should be used in making comparisons between modeled and measured data). The general rank order of receiver height was predicted correctly by the model, as

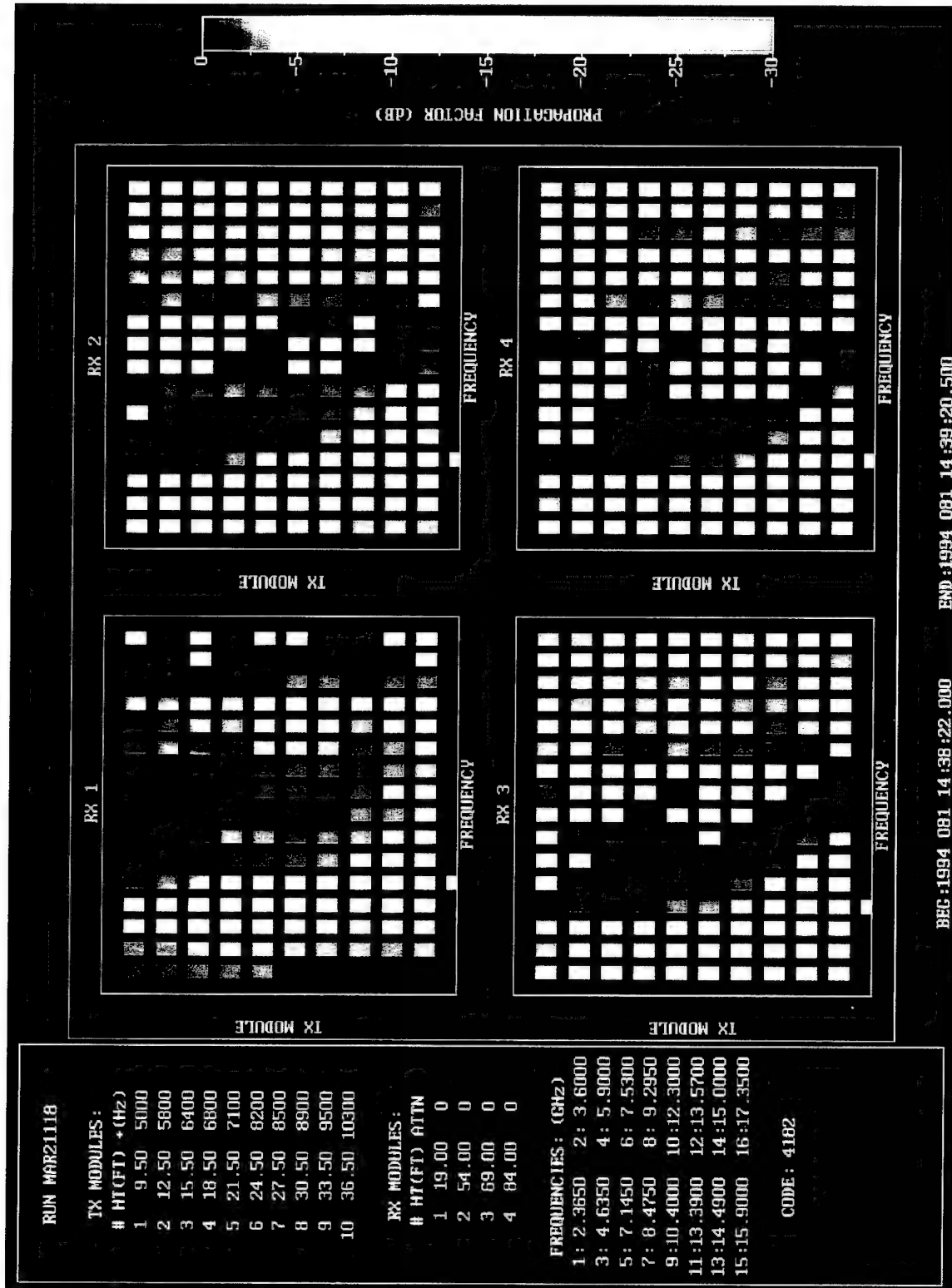


FIGURE 4-6. STATIC PLOT 22 MAR 94 14:38 UTC

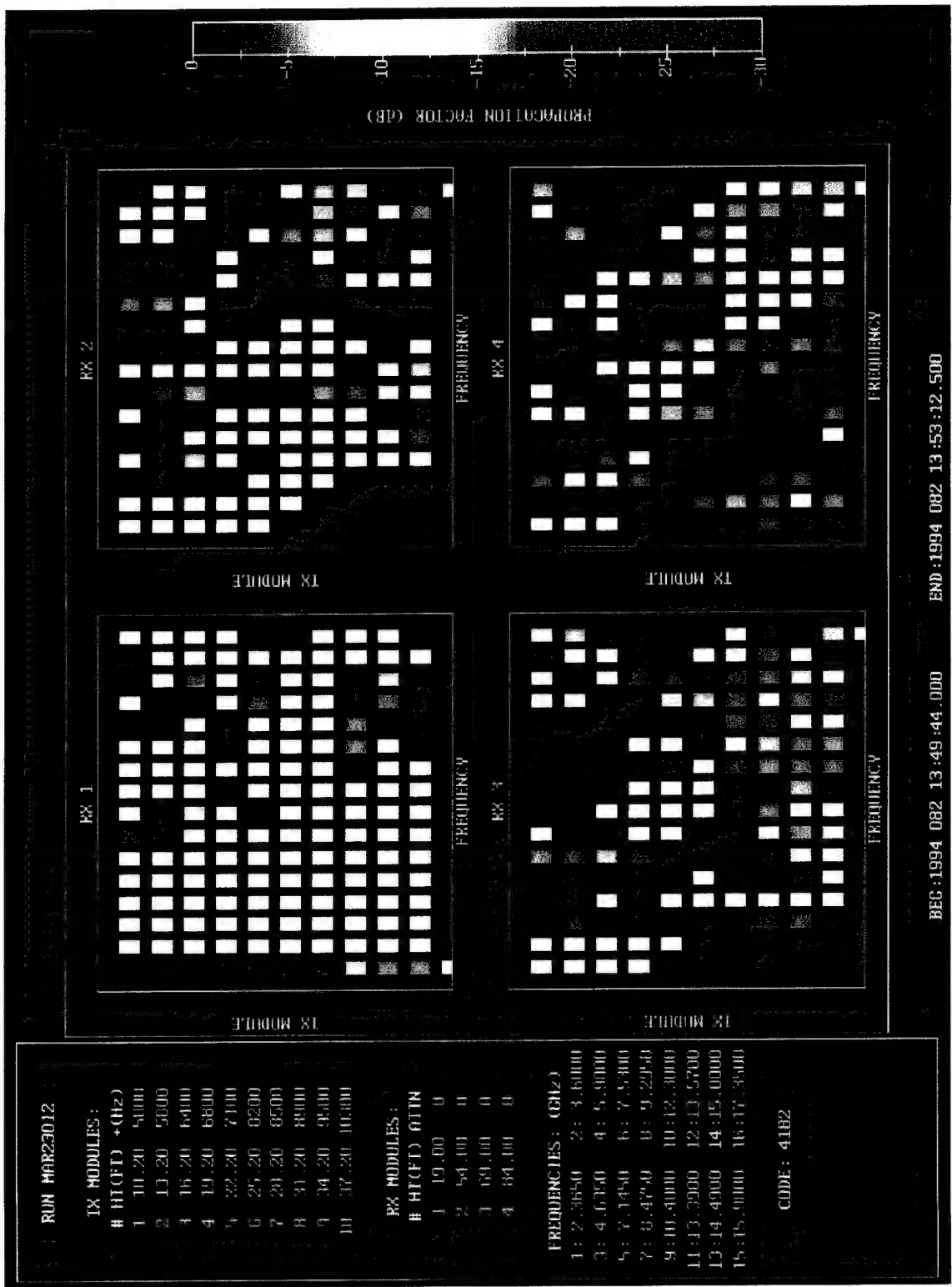


FIGURE 4-7. STATIC PLOT 23 MAR 94 13:49 UTC

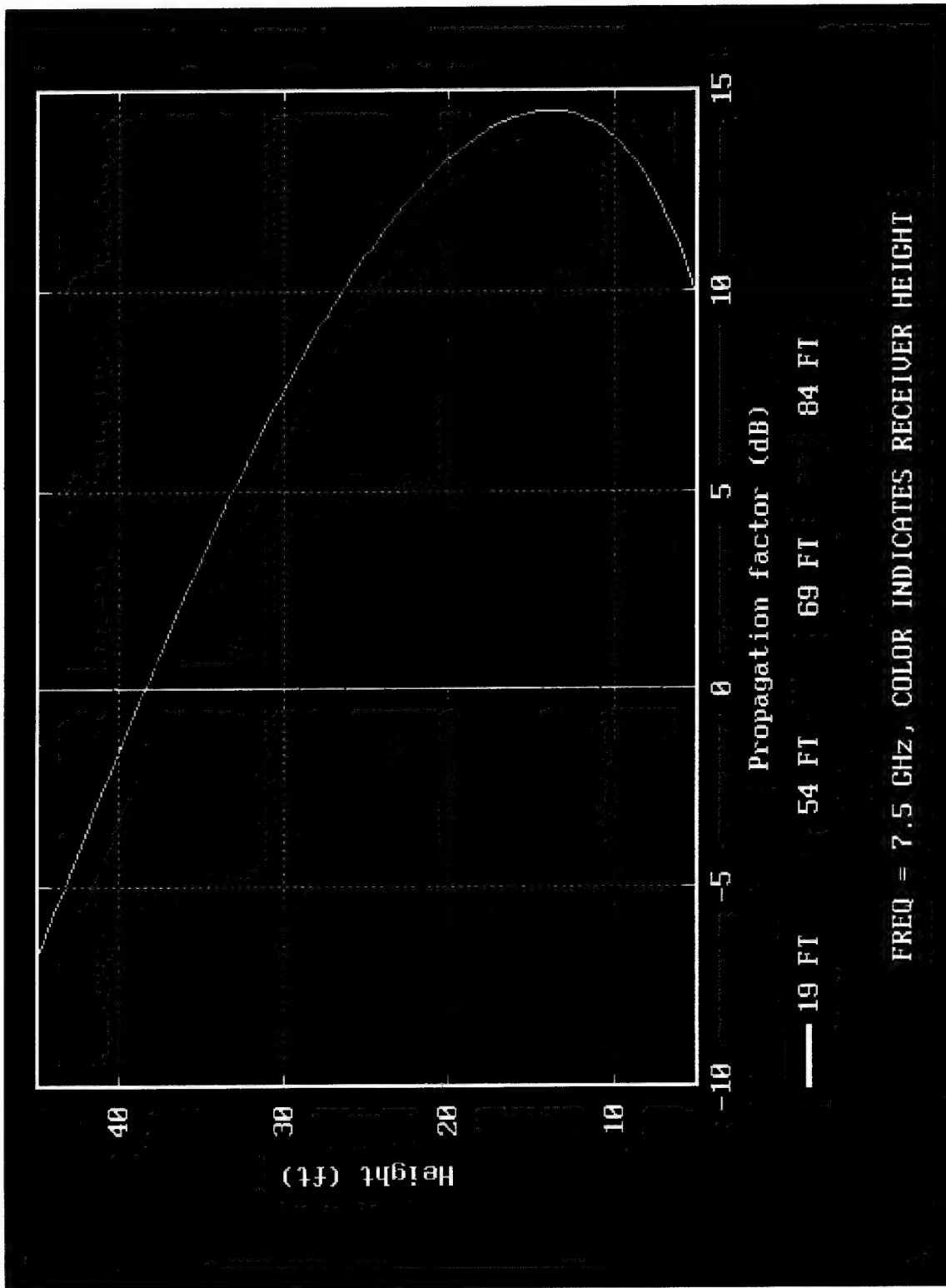


FIGURE 4-8. MODEL OUTPUT 23 MAR 94 RUN 1 PROFILE 1

were the values for the peaks or heights of least loss for the range of the MPMS transmitters; however, the modeled pathloss shows null structure at different heights than the measured data show. Figure 4-9 shows the model output for the 22 March case (compare with measured data shown in Figure 4-6), again for Frequency 6. Neither the measured data nor the model output showed null structure versus height. The loss values for the modeled and measured curves were close, and the general rank order of the receivers with respect to these values agrees between the modeled and measured data. The height at which the measured data from Receivers 2, 3, and 4 show less than 0 dB loss relative to free space (note white data points) does not occur at the height predicted by the modeled output; however, the agreement between the two is otherwise fairly close considering the amount of available refractive profile data. The dominant type of ducting present on 22 March at 14:39 UTC appeared to be an evaporation duct of about 34 ft. On 23 March at 13:53 UTC, the dominant ducting feature appeared to be a surface-based duct of about 55 ft that spanned 7.5 M units (modified refractivity units). Figures 4-10 and 4-11 show the refractive profile inputs used for the modeled data plots of Figures 4-8 and 4-9, respectively.

## VERTICAL NULL VARIABILITY

Figure 4-12 is a "dynamic" plot, which uses color to indicate propagation factor relative to free space versus time for a single frequency for the four receivers. Receiver 4 is at the top. The vertical axes indicate transmitter height. Time is along the horizontal axes, which in the majority of cases will cover 8 min or 480 sec as stated in the upper left of the graph. Begin and end times are listed at the bottom of the graph and total run time is listed at the top. Only one frequency is plotted, and that frequency is indicated by the white marker at the top of the graph.

The "dynamic" plot in Figure 4-12 is of Frequency 14 (15.0 GHz) for the 8-min period included in that data collection interval on 23 March 94 at 07:01 UTC. The diagonal lines of yellow and blue tones flanked by diagonals of orange, red, and white show periods during the 8 min where a null and peak structure moved from approximately 7 ft to 34 ft in an increasing progression with time. This pattern is repeated at least three times for Receiver 4 with each diagonal covering about 1.5 min; the pattern is repeated once for Receiver 2 with the diagonal covering about 2.7 min, and once for Receiver 3 with a diagonal much like those that appear in the graph of Receiver 4. Only a ragged representation of the diagonals is shown for Receiver 1.

Figures 4-13, 4-14, and 4-15 are "frequency line" plots of data from the same time period as Figure 4-12, for 3.6, 8.475, and 15.0 GHz, respectively. These plots show an increase in null structure with increasing frequency, as well as the overplotted time history or variability of these three frequencies across the band covered. At the lower frequency, the profiles "fan" in a smooth fashion with time, changing direction from left to right and back in an undulatory fashion over the 8-min interval shown. The character is actually much more evident when the plots are seen through video as they progressed with time. A more jagged profile is evident for the 8.475-GHz data in Figure 4-14, showing how higher frequencies are affected by the same ducting environment; the profiles for 15.0 GHz (Figure 4-15) show a further increase in null structure with height (note that these are the same data as are covered in Figure 4-12 in the "dynamic" plot format). These nulls vary as much as 30 dB over the 8-min interval in some cases. Since these data were collected over a one-way path, the variability for a two-way system like a radar would be more than 60 dB. For all three



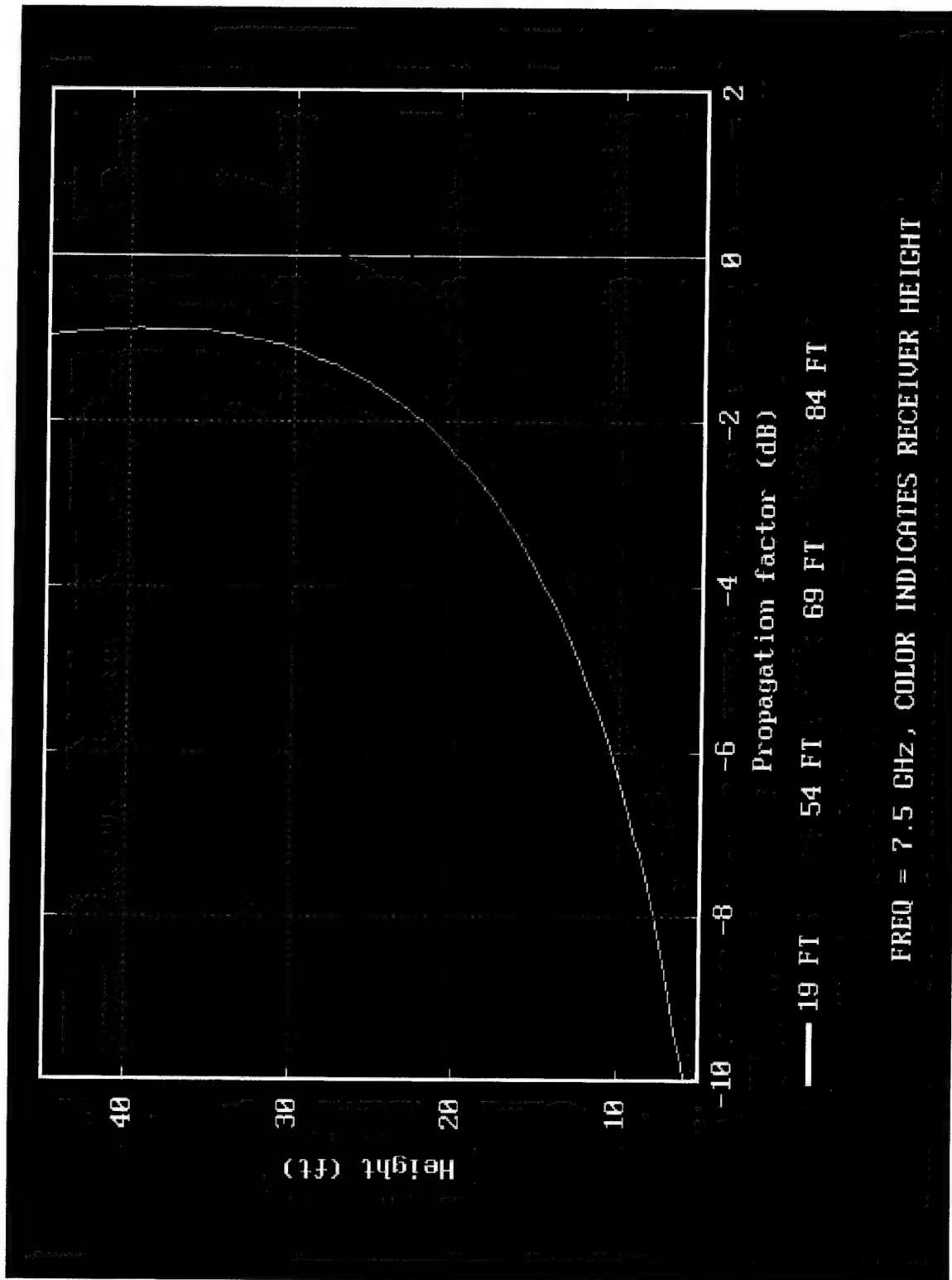
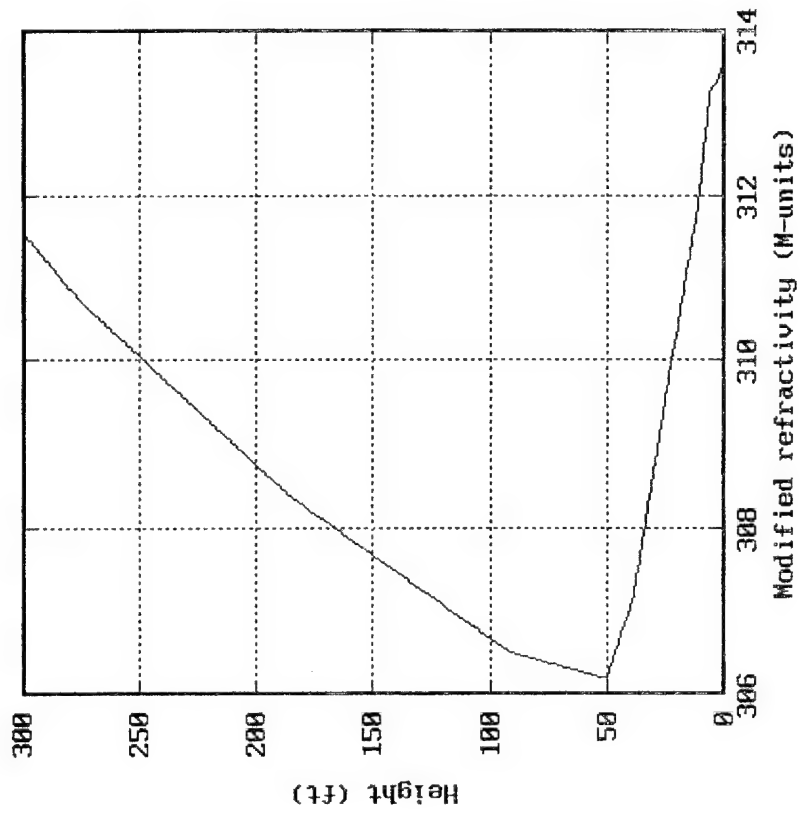
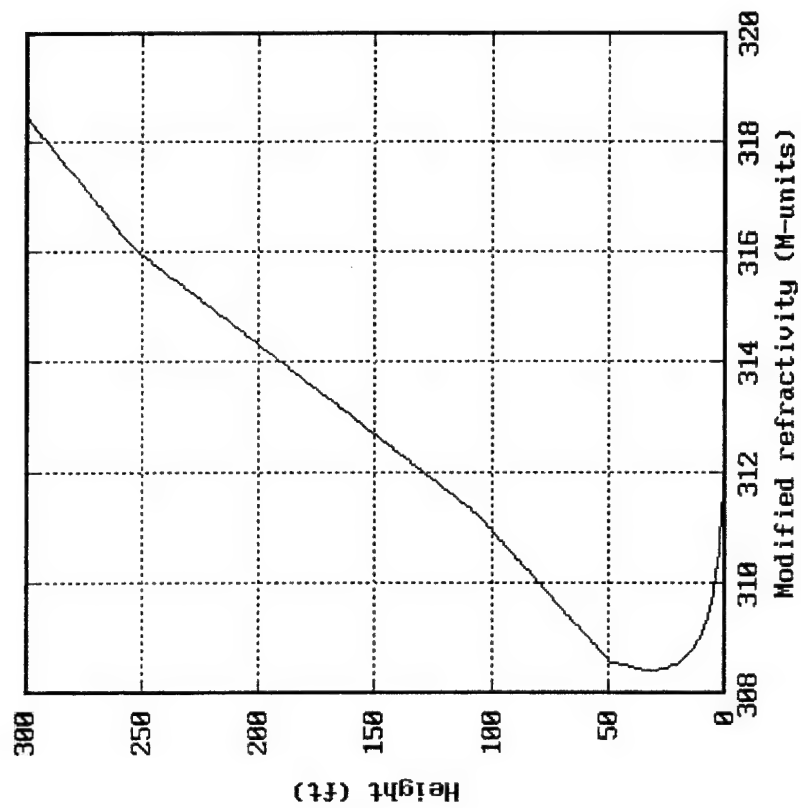


FIGURE 4-9. MODEL OUTPUT 22 MAR 94 RUN 2 PROFILE 1



REFRACTIVE PROFILE 1 HELD RUN 1 MAR 23 AT 1320-1342 Z

FIGURE 4-10. REFRACTIVE PROFILE 23 MAR 94 RUN 1 PROFILE 1



REFRACTIVE PROFILE 1 HELO RUN 2 MAR 22 AT 1420-1451 Z

FIGURE 4-11. REFRACTIVE PROFILE 22 MAR 94 RUN 2 PROFILE 1

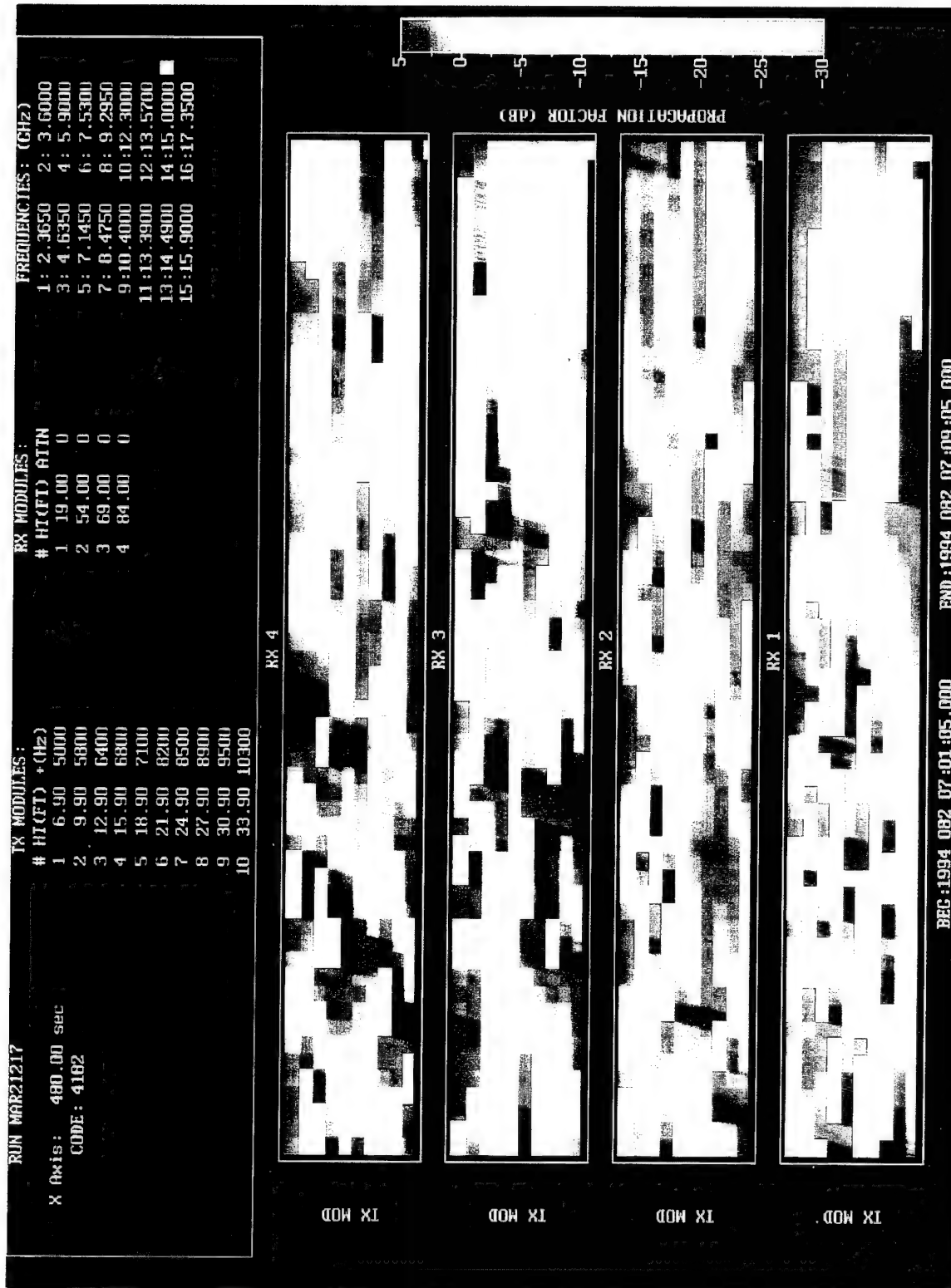


FIGURE 4-12. DYNAMIC PLOT 23 MAR 94 07:01 UTC

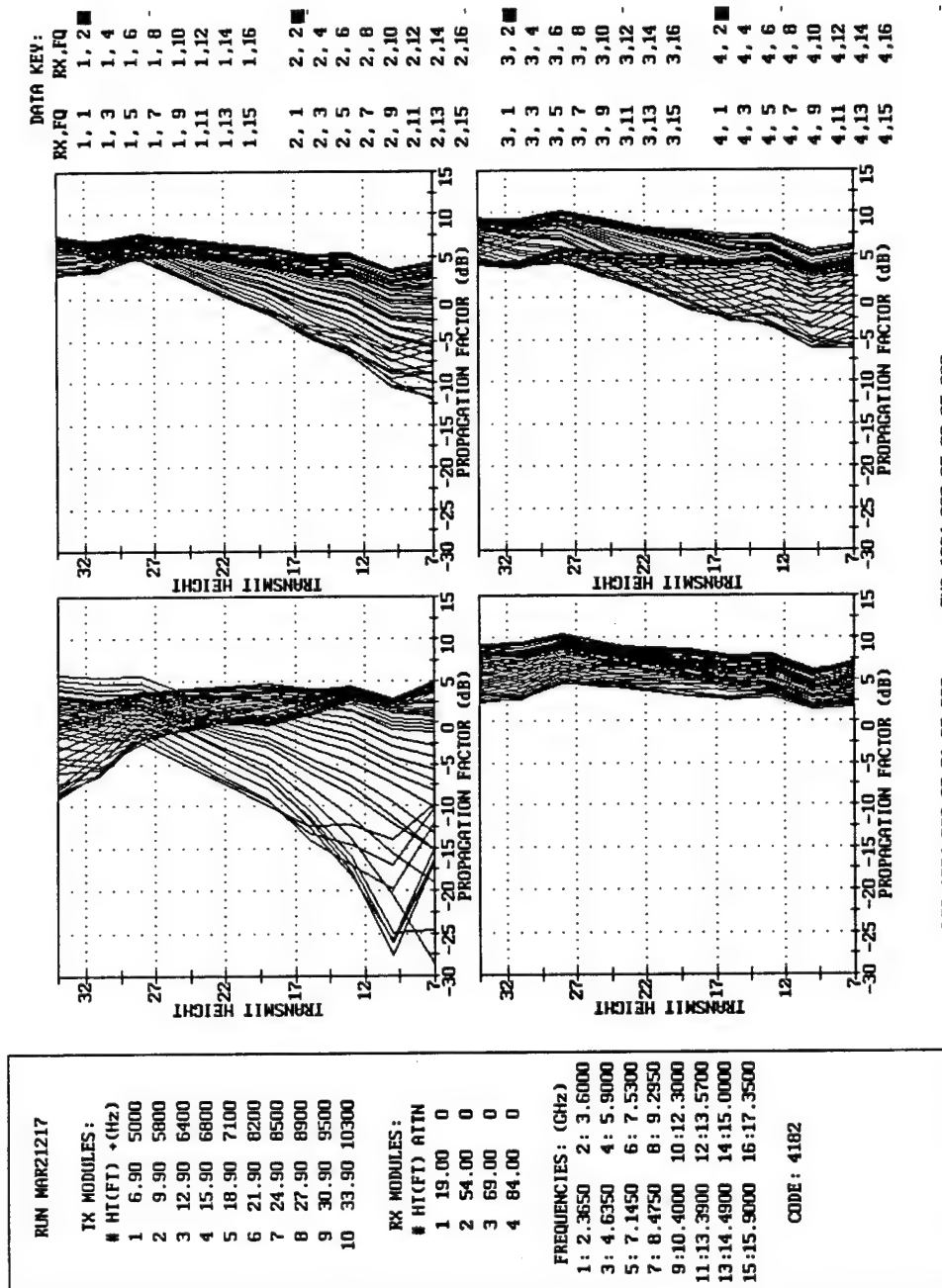


FIGURE 4-13. LINE PLOT, 3.6 GHZ, 23 MAR 94 07:01 UTC

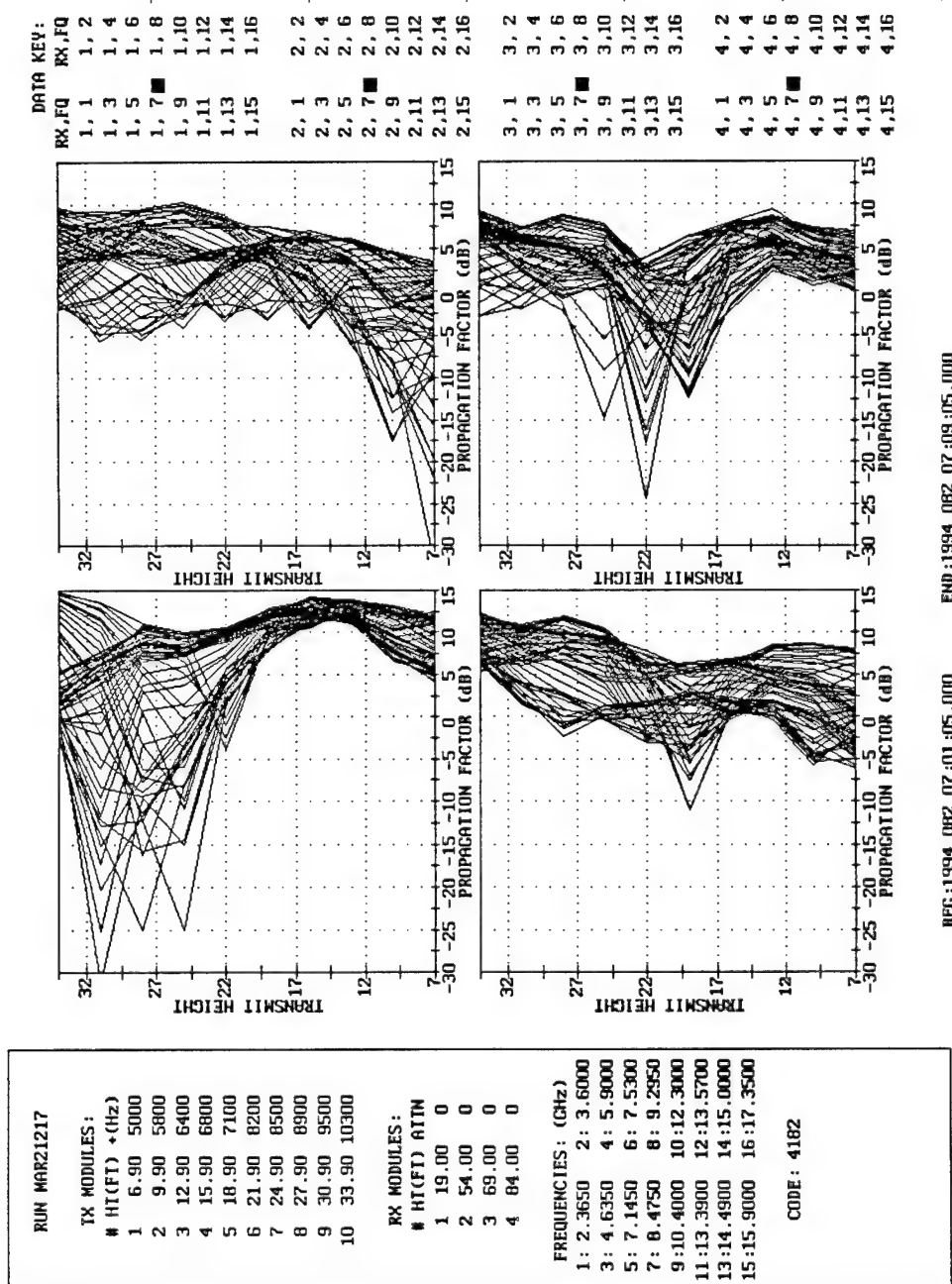
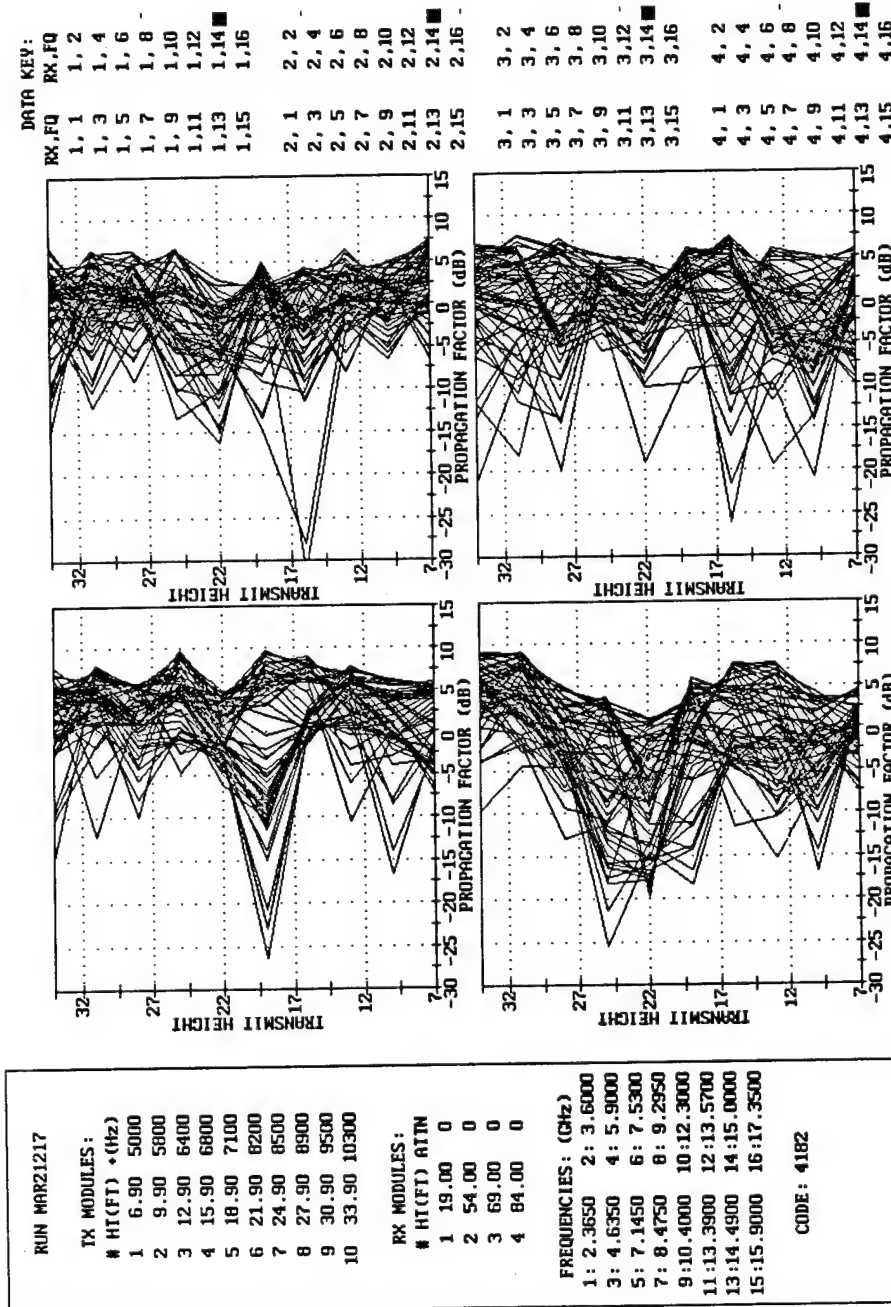


FIGURE 4-14. LINE PLOT, 8.475 GHZ, 23 MAR 94 07:01 UTC



BEG:1994 082 07:01:05.000      END:1994 082 07:09:05.000

FIGURE 4-15. LINE PLOT, 15.0 GHZ, 23 MAR 94 07:01 UTC

frequencies, propagation was quite good overall, indicating a fairly strong duct, with low frequencies and low altitudes all showing propagation enhancements over standard atmosphere of at least as much as 10 dB (one way), and in some cases, as much as 50 dB.

Figure 4-16 is a "dynamic" plot from the same day as shown in Figure 4-12, but approximately 30 min later. The amount or strength of the ducting present appears to be lessening, and the diagonals for this data segment slope downward with time and aren't as steep. The meteorological data available for both of these events do not include helicopter refractive profiles because of the time of day (around 2 a.m. local time). The local meteorological parameters indicated fairly cold temperatures of about 6 C, moderate relative humidity of about 75 percent, and light winds at about 4 kn. The brief fade in propagation which followed these plots lasted only approximately 20 min, and none of these meteorological parameters changed significantly.

Figure 4-17 is a "dynamic" plot which shows periods where null variability was very minimal with time. Figure 4-17 was about 5.5 hr after the period shown in Figure 4-6 where there was an obvious enhancement in signal strength for the higher receiver heights. The frequency shown in this plot, 8.475 GHz, is about midband for the system and shows no such enhancement; in fact, the lowest receiver altitude seems to be slightly favored. Also, very little null structure with transmitter height is evident for any of the receivers. The meteorological data for this time period indicated an evaporation duct height of 69 ft that was increasing in height with time. The propagation model output shown in Figure 4-18, which was derived from the profile taken by the helicopter nearest to shore and nearest in time to the data in Figure 4-17, underestimated the signal strength for the three higher receivers and overestimated the signal strength for the lowest receiver. The general rank order of best-to-worst receiver loss was a match between the measured and modeled data, at least for some heights. Since the refractive information for the entire Parramore path was not available, part of the differences between the measured and modeled output could be attributed to that discrepancy. (Figure 4-19 shows the refractive profile that was used as input to the propagation model output shown in Figure 4-18.)

Figure 4-20 is another dynamic plot from the same day as Figure 4-17, but another 2.75 hr later. The dynamic plot in Figure 4-20 also shows a period where null variability was minimal with time. A striking preference for the lowest receive antenna altitude is evident with propagation factor values as high as +15 dB relative to free space at a transmitter height of about 14 ft. Well established nulls at about 20 to 23 ft, which were also time invariant over the 8-min period, are evident in the three highest receivers. The signal level is approximately 25 dB lower in these null regions. This plot shows a complete reversal of the character shown in Figure 4-6 some 8 hr earlier. As stated above, the meteorological data indicated an increasing evaporation duct throughout the day. The refractive data last collected (depicted in Figure 4-19) coincided with Figure 4-17 and were taken 2.75 hr earlier than the data shown in Figure 4-20.

Comparison of the measured data in Figure 4-20 with the null structure predicted by the propagation model in Figure 4-18 shows some agreement for the two highest receivers, but an approximate 5-ft difference for Receiver 2. The levels of the peak values versus height match quite well between the modeled and the measured data for the lowest receiver, with values at about +12 dB and +14 dB, respectively, relative to free space. Levels of peak values versus height match less well



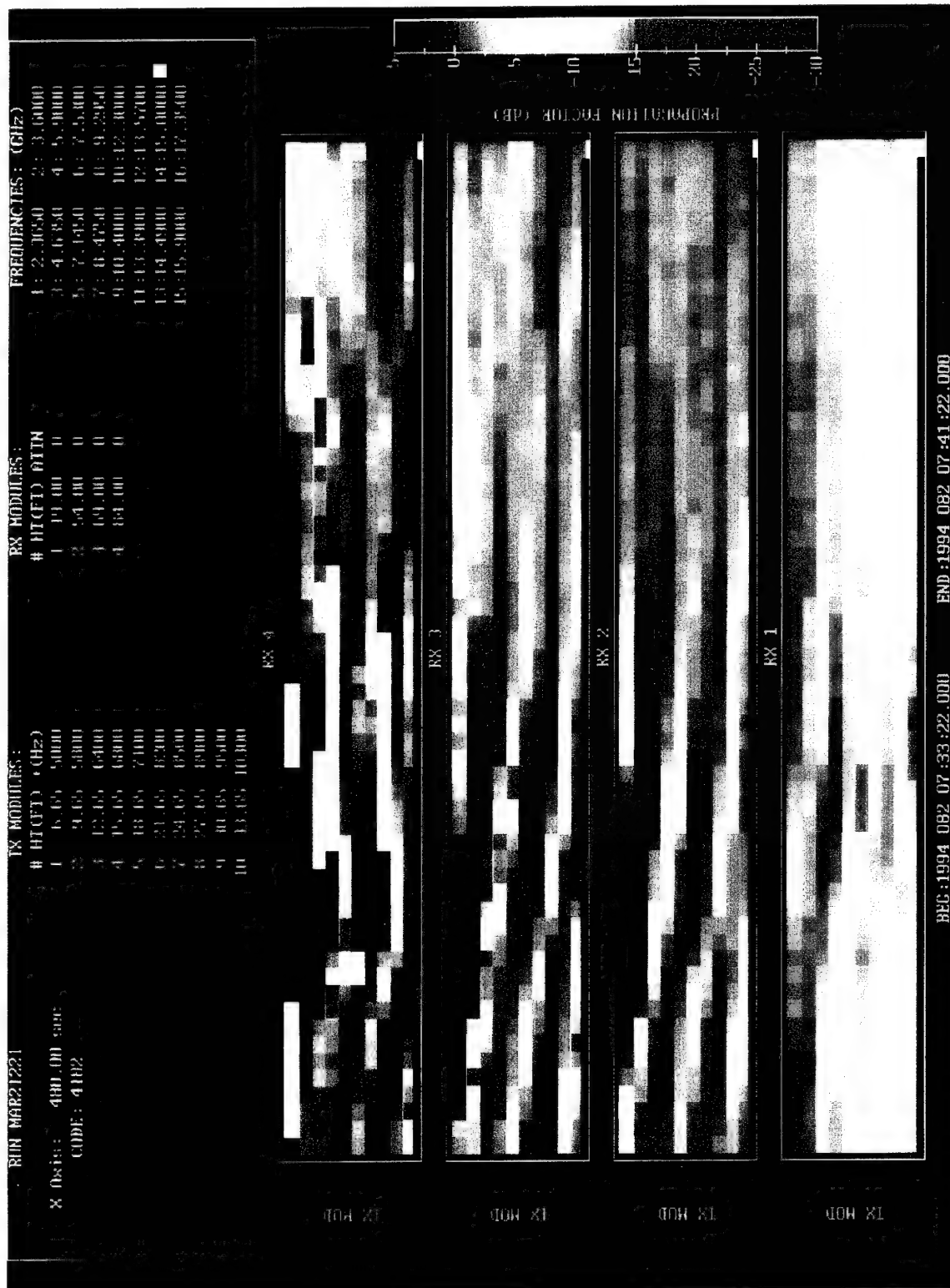


FIGURE 4-16. DYNAMIC PLOT 23 MAR 94 07:33 UTC





FIGURE 4-17. DYNAMIC PLOT 22 MAR 94 19:54 UTC

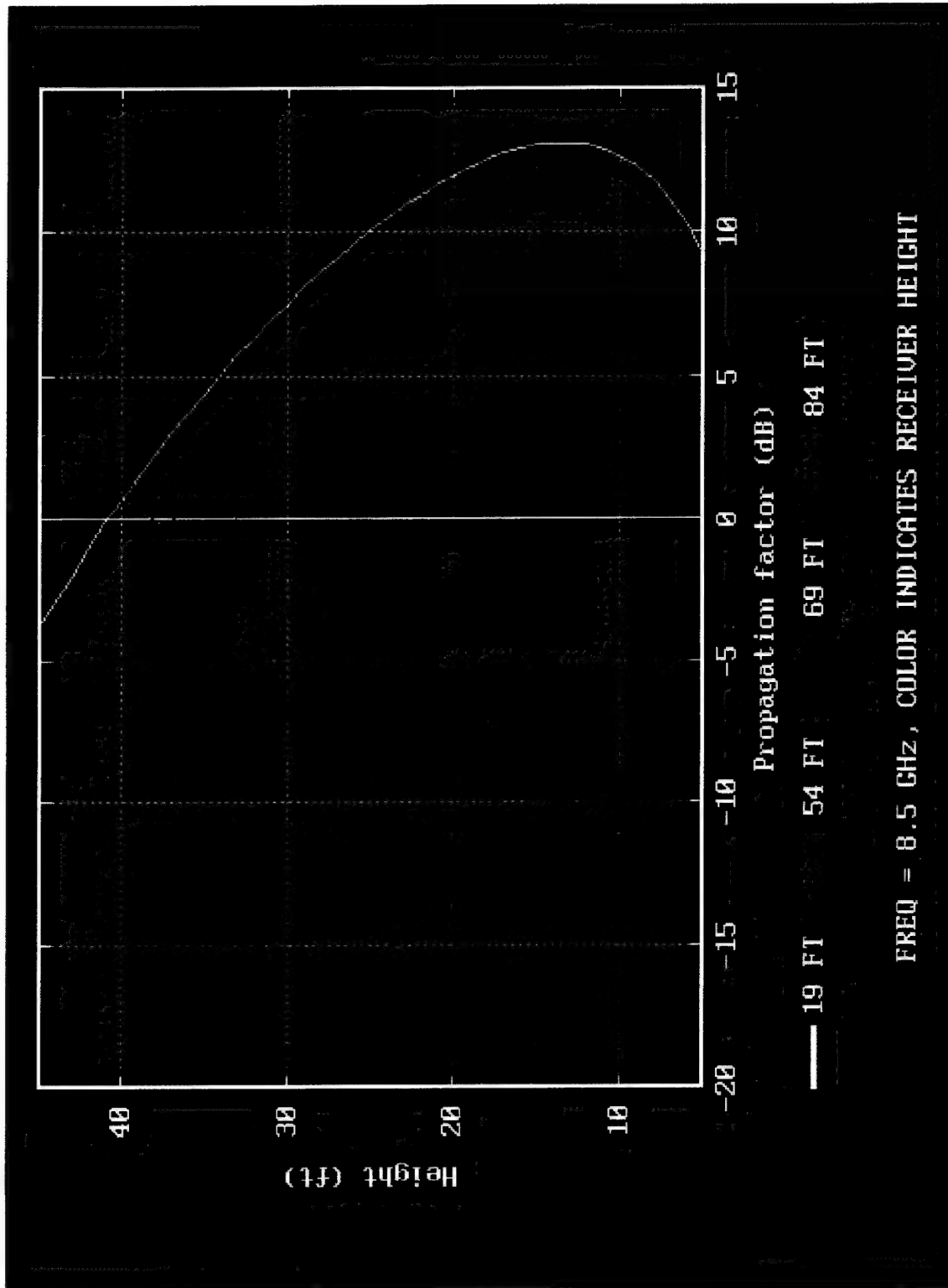
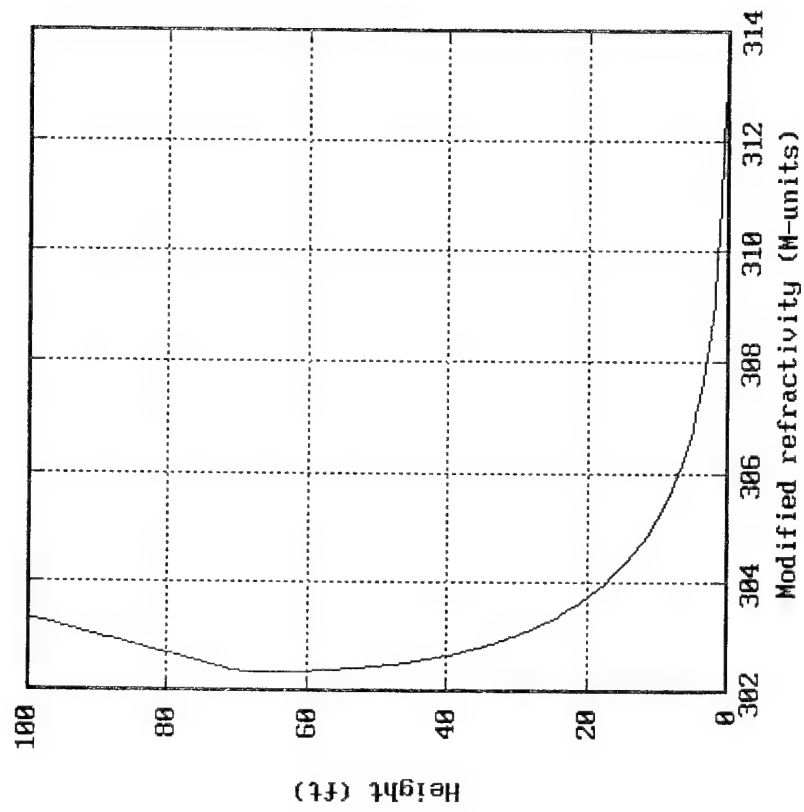


FIGURE 4-18. MODEL OUTPUT 22 MAR 94 RUN 5 PROFILE 1



REFRACTIVE PROFILE 1 HELD RUN 5 MAR 22 AT 1936-2006 Z

FIGURE 4-19. REFRACTIVE PROFILE 22 MAR 94 RUN 5 PROFILE 1



FIGURE 4-20. DYNAMIC PLOT 22 MAR 94 22:44 UTC

for the higher three receivers with differences around 5 to 10 dB. Since the modeled output in Figure 4-18 was derived from data collected some 2.75 hr earlier than the data shown in Figure 4-20, the agreement between the modeled and measured data is good.

#### FREQUENCY EFFECTS ON NULL FILLING

Much of the data collected are useful in analyzing the percentage bandwidth necessary to mitigate or "fill in" null structures in the pathloss profiles created by multimode propagation in ducting environments.<sup>4</sup> Figure 4-21 illustrates this effect using some of the data collected. The data shown in Figure 4-21 were taken during a ducting environment and cover 1 min, with the data collected during this minute overplotted. Only the data from Receiver 2 (approximate height above mean sea level was 54 ft) are shown for four frequencies, 5.9, 8.475, 13.57, and 17.35 GHz (one frequency per graph, from left to right, top to bottom). The data show an increase with frequency in the number of nulls as well as a shift in the heights of these nulls with a change in frequency. The data cover only from about 7 to 34 ft however, and structures above and below these heights were not measured. The lowest frequency shown in these graphs (5.9 GHz) appears to have the best overall loss performance and no large null structures; however, the data do not show any values above 34 ft, and it is likely that a significant null was present at some height between 34 and 100 ft for this frequency as well. The exact height of the nulls is dependent on the refractive profiles in effect at the time the data were collected. These effects or null structures also occur with range, which was not measured by the system during these tests since all data were collected with both terminals fixed. Theoretical analysis has shown that within the multipath region (inside the radar horizon), frequency diversity could be used to fill multipath nulls effectively for any refractive environment. A follow-on task involves the use of the MPMS with the transmitter tower on a moving platform. The data collected during this experiment could be used to verify this effect. Figure 4-21 shows that a significant change in carrier frequency significantly alters where null structures occurred versus height; however, Figure 4-1 shows that for Receiver 3, a null was present at approximately the same height for all of the higher frequencies (12.3 to 17.35 GHz). A complete study focused on just this effect for the entire test period would help to quantify both the percentage bandwidth necessary to fill nulls and the percentage of time the refractive environment was such that frequency diversity could be used to improve overall loss performance.

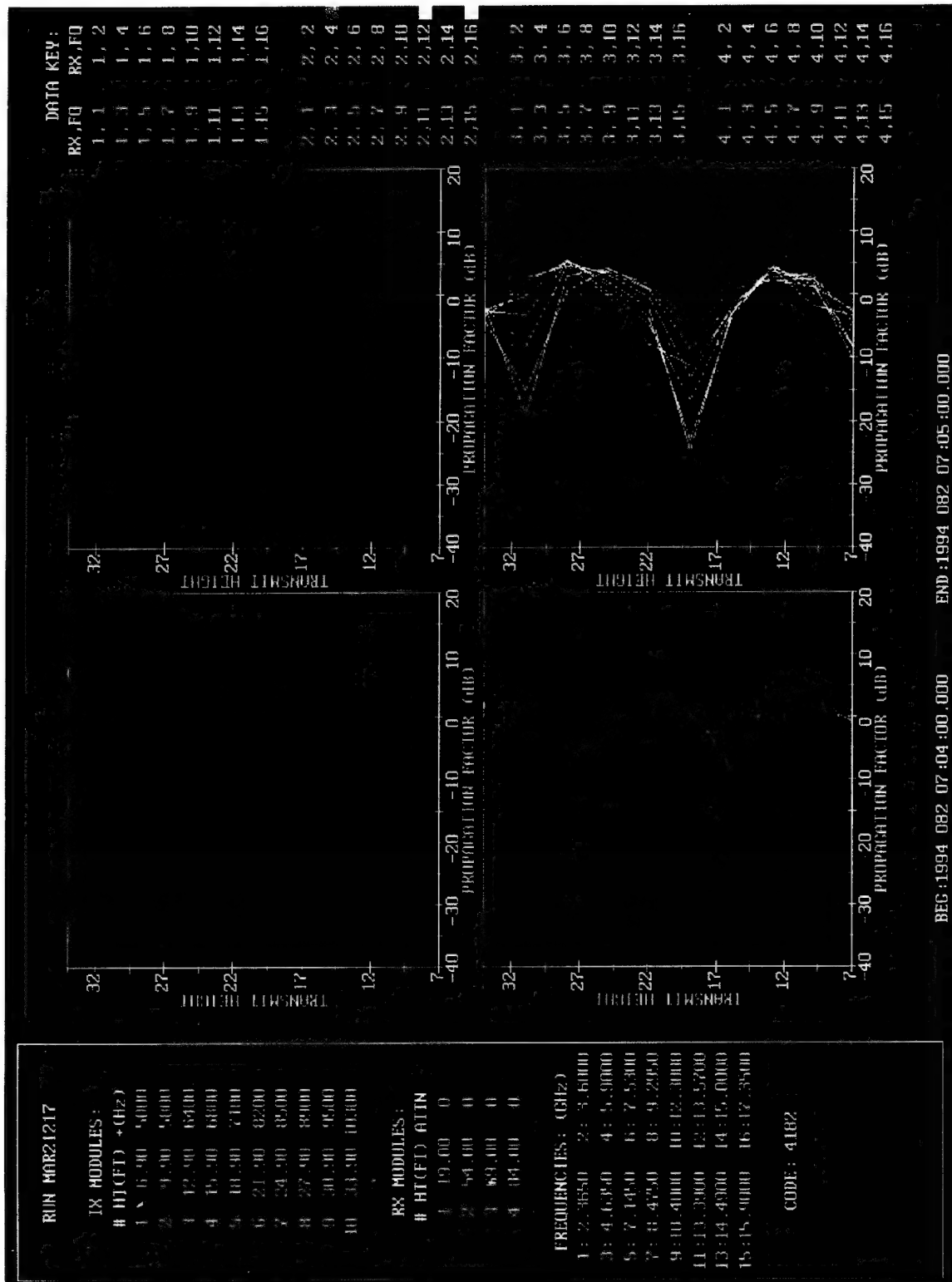


FIGURE 4-21. LINE PLOT 23 MAR 94 07:04 UTC; 5.9, 8.475, 13.57, 17.35 GHZ



## SECTION 5

### SUMMARY AND GENERAL OBSERVATIONS

The MPMS was moved to Wallops Island in December 1993 to participate in the Multisensor Integration (MSI) Test. The basic soundness of the system was established at Dahlgren, but the operational period was inadequate for a thorough evaluation. Consequently, weaknesses that required software modifications were revealed during the test. Nevertheless, after initial operation was established on 4 February 1994, MPMS was online, often around the clock, for a large fraction of the test period and provided valuable online insight on RF propagation, both during specific tests and during nontest times. Within the limitation of operating over a fixed range, MPMS performance met all expectations. Significant data were recorded for prolonged periods of both very good and very bad propagation as well as for transitions between the extreme conditions. For the first time, RF propagation structure was measured and recorded at a high sampling rate, across a broad frequency span simultaneously for a mix of heights at the two terminals, and under a wide range of propagation conditions. These recordings will be valuable in evaluating questions of RF frequency choice and operational frequency management. For the times when IR measurements were made over the same fixed range, the recorded RF data will be used to assess combined RF/IR performance. The following are general observations on propagation as seen by the MPMS.

#### FREQUENCY

In general, the mid frequency range, 5.9 to 12.3 GHz (with 7.5 GHz perhaps being the best) showed the least loss over all conditions viewed to date and the least variability with time and transmitter height. The profiles of loss versus transmitter height were more uniform for these frequencies, suggesting that for the environmental conditions experienced during these tests, radar performance would be independent of target height at least for heights between 7 and 35 ft. This observation was especially true for strong ducting conditions where multimode effects dominated higher frequency performance causing dynamic null structures with transmitter height and time. The data collected are a valuable asset for evaluating radar frequency management schemes designed to mitigate the effects of high loss nulls.

#### RECEIVER HEIGHT

The receiver height did affect the measured pathloss differently depending on the refractive environment. Under certain strong ducting situations the lowest receiver showed both the least loss and significant enhancements in signal strength (+15 dB relative to free space one-way) for some transmitter heights. In general, when propagation was standard atmosphere or worse (subrefractive),

the highest receiver height was favored. The mid-height receivers were favored on one observed occasion during the week described in this report. The data collected are pertinent to assessing the radar benefits accruing from height diversity.

## TRANSMITTER HEIGHT

The transmitters in this data collection represented target altitudes from about 7 to 35 ft. Tide fluctuations were measured and recorded with time so that the transmitter heights could be adjusted accordingly. The plots shown in this report include tide effects. The vertical null structure with transmitter height was variable, but in general increased with increasing frequency and duct height, as predicted by propagation models. The exact location of these nulls was not always predicted well by the propagation models, but their presence in the data was. The nulls did not seem to favor any one transmitter altitude. Some nulls were narrow enough in height that more closely spaced transmitters would be required to resolve the null structure.

## TEMPORAL VARIABILITY

The data collected during this test exhibited both short-term and long-term temporal variability. An example of the long-term variability was discussed in Section 4 ("Transition From Ducting To Subrefraction") where those transitions took place over 2.5 hr, approximately, and lasted for over 30 hr in one state. During the ducting periods the short-term variability was most evident; the variations in null structure routinely produced significant changes in both the height of the null (e.g., null shifts of 6 ft in 8 sec) and depth of the null (e.g., depth changes of 15 dB in 16 sec). These short-term variations were most evident at the higher frequencies; i.e., 8 GHz and above; however, even 3.6 GHz showed significant variability over 8 min as shown in Figure 4-13. Conversely, the strong ducts like the one responsible for Figure 4-20 produced very tight profile structures with time, with as little as 2 dB of spread over an 8-min interval (for the lowest receiver), even though the signal enhancement was nearing +14 dB at the peaks, indicating a very strong degree of trapping. From the available meteorological data, it seems that strong, well-formed evaporation ducts cause less short-term variability than do other types of strong surface-based ducts. Also the variability of these evaporation ducts with time is probably slower than the other types of surface-based ducts, which may be caused by air masses moving from land to water.

## METEOROLOGICAL DATA AND MODEL PREDICTIONS

The propagation models used in the above analysis suffered in their ability to predict the measured data because data taken at concurrent times and along concurrent paths were unavailable. The overall test, of which these propagation measurements were a part, had priority and safety issues that often precluded the collection of the helicopter profiles along the path of interest to Parramore Island. The helicopter-generated profiles coupled with the evaporation duct measurements are believed to be the best input data for the propagation models, since they include range-dependent effects; however, these profiles are made on only one radial at a time. Often other test operations requiring the helicopter profiles occurred on a radial outbound from the coast, whereas the MPMS

data were collected along a path just off the coastline to Parramore Island. Also, many of the interesting features in the data occurred at a time of day when most personnel were not available. Since the MPMS was designed to collect data around the clock, many such occasions exist in the database. The dynamic nature of the meteorological environment, both in space and time, continues to present difficulties in the collection of a meteorological data set sufficient to adequately drive the propagation models. Overall, gross features in the measured propagation data were borne out by the propagation models, with detailed matches being obtained less often.

#### DUCTING ENVIRONMENT

For the time period covered by these tests (from January through April 1994) a significant amount of strong ducting was observed, as well as several periods of severe subrefraction. Even during cold weather, ducting occurred for a substantial percentage of the test period.

## SECTION 6

### FUTURE MEASUREMENTS

This test of the MPMS was its first, and as such, could be improved upon. Certainly a few months of data collection in one location during one season of the year does not show all the significant features of low altitude propagation that are of interest. However, the primary goal for the MPMS was first to support the MSI Test in terms of providing a propagation reference for the sensor data that were being collected; the general assessment of low altitude propagation characteristics (or database enhancement) was a secondary goal. More data collections are planned as the system is used in conjunction with other test efforts. Plans are also being made to mount the MPMS transmitter array on a boat capable of about 20 kn to collect data over a range-varying path. Ultimately, the MPMS provides a completely unique capability to measure propagation for low elevation targets with fine height and frequency resolution covering most of the shipboard radar frequency band. With future upgrades and more data collection efforts during different times of the year in different locations, the data collected have the potential to show features that have yet to be measured with certainty by any system and to provide a comparison of these features across time, height, range, and frequency. These data should be invaluable input to the design of future horizon search-and-track Navy radars.

## SECTION 7

### CONCLUSIONS

The measurements of RF propagation described in this report have shown that the propagation environment varies significantly with altitude, range, time and frequency. Over 15 dB of variation in one-way propagation loss was observed for target height differences of 3 ft or time periods of less than 20 sec. This variation would be double for a two-way system like a radar, and would likely lead to significant detection performance variations. Longer term variations from ducting to subrefractive environments that resulted in a 40 dB change in one-way loss were also observed. These subrefractive environments lasted over 30 hr in some cases, and the loss values were essentially frequency-independent over the 2 to 18 GHz band. Only increasing the height of the radar receiver showed any decrease in the pathloss during these subrefractive conditions.

The data indicate that most conventional narrow band radars will be subject to a significant amount of performance variation in the detection of sea-skimming threats. Radars with the capability to use a wide range of carrier frequencies could average out these variations. Ducting also affects the level of surface clutter returns, so that the radar must necessarily be designed with adequate flexibility to adapt its waveforms for the environment.

The propagation models used for comparison with the measured data in this report often produced results that were somewhat representative of the environment measured; however, detailed comparisons were nearly always lacking. The models suffered in many cases because of the lack of temporally and radially coincident refractive profile data. Even when the best possible refractive profile data were available, the small-scale temporal variations present in the measured propagation data indicated that detailed direct comparisons could show favorable results only for the most temporally stable cases.

Because of the complexity of the low elevation propagation region, radars designed to detect the sea-skimming threat must necessarily have a high degree of flexibility, both in frequency coverage and waveform characteristics, to cope with performance variations caused by the natural environment.

## SECTION 8

### REFERENCES

1. Stapleton, J., "Refractivity Measurements Using A Vertical Array of Temperature and Humidity Sensors," Naval Surface Warfare Center, Dahlgren Division *Technical Digest*, September 1992.
2. Goldhirsh, J., and Dockery G., "Propagation Measurements and Modeling at C band for Over-the-Water, Line-of-Sight Propagation Links in the Mid-Atlantic Coast," *Radio Science*, Vol. 26, Number 3, May-June 1991.
3. PCPEM [Personal Computer Parabolic Equation Model] © 1989, 1990 of Signal Science Limited.
4. Dockery, G. D., *Propagation Fade Characteristics in Low-Altitude Surface Ducts*, Technical Report, Task 3-1-19, The Johns Hopkins University, APL, Oct 1988.

**APPENDIX A**  
**EQUIPMENT DESCRIPTION**

## MICROWAVE PROPAGATION MEASUREMENT SYSTEM (MPMS)

The MPMS consists of 10 transmitters and 4 receivers, which are used to transmit and receive continuous wave (CW) radio-frequency signals. The power received is used to determine one-way propagation loss using transmit and receive calibration data. The system is capable of transmitting any frequency in the 2 to 18 GHz band with 1-kHz resolution, although the direct digital synthesizer (DDS) discussed in the following paragraphs allows much closer frequency resolution than this basic value. In general, this frequency band is covered in 16 frequency steps in 8 sec. The system has a variable frequency switching rate of 0.5, 1, and 2 Hz. The system can be set up to collect data continuously for an extended period of time to observe the temporal variation of propagation profiles. The system collects data on radio frequency (RF) transmit power, RF received-signal power, the time of data collection, and various other system monitor parameters necessary to determine calibration and system performance.

The 10 individual transmit modules are mounted on a 30-ft tower and spaced 3 ft apart to the center of each transmit aperture. The receive modules are mounted on a 100-ft tower at heights of 19, 54, 69, and 84 ft nominally, with at least  $\pm 5$  ft of adjustment in height possible. The 4 receivers receive the RF signal transmitted by all 10 transmitters, simultaneously, using 4 parallel receive channels. The frequency of each transmitter is offset slightly (300 to 1000 Hz) from the other transmitter frequencies so that the individual transmitter heights are separable using spectral analysis of the received signals.

The frequency offset on each transmitter is achieved by taking the output of the synthesized signal generator and mixing it with the output of a DDS as shown in Figure A-1. Both the signal generator and the DDS are controlled by the main computer via a GPIB or RS-232 interface. The 5-MHz reference signal is derived from a highly stable, low-phase-noise oscillator that is part of the Global Positioning System (GPS) receiver. The 5-MHz reference signal is then doubled to 10-MHz to lock the synthesized signal generator and the DDS. The 10-MHz signal source into each DDS is tripled to 30 MHz to enable the DDS to produce a maximum output signal of 15 MHz. By setting the signal generator 10 MHz lower than the selected carrier frequency and mixing with the DDS frequency,  $10 \text{ MHz} + N \text{ Hz}$ , the output signals  $f_o - 20 \text{ MHz} + N \text{ Hz}$  and  $f_o + N \text{ Hz}$  are obtained. The single sideband modulator is optimized for the upper sideband,  $f_o + N \text{ Hz}$ .

The signal is amplified further and transmitted through a horn antenna. A directional coupler is used directly before the antenna to feed a diode detector whose output is in turn fed to an Analog-to-Digital (A/D) converter. The A/D output is calibrated to constantly monitor the power transmitted by each transmitter. During the transmitter calibration, a power meter is used to verify that these power-monitor values are correctly determining the transmitted power. The power-monitor values are telemetered back to the receiver base station and are recorded and used in the display of the collected pathloss values.



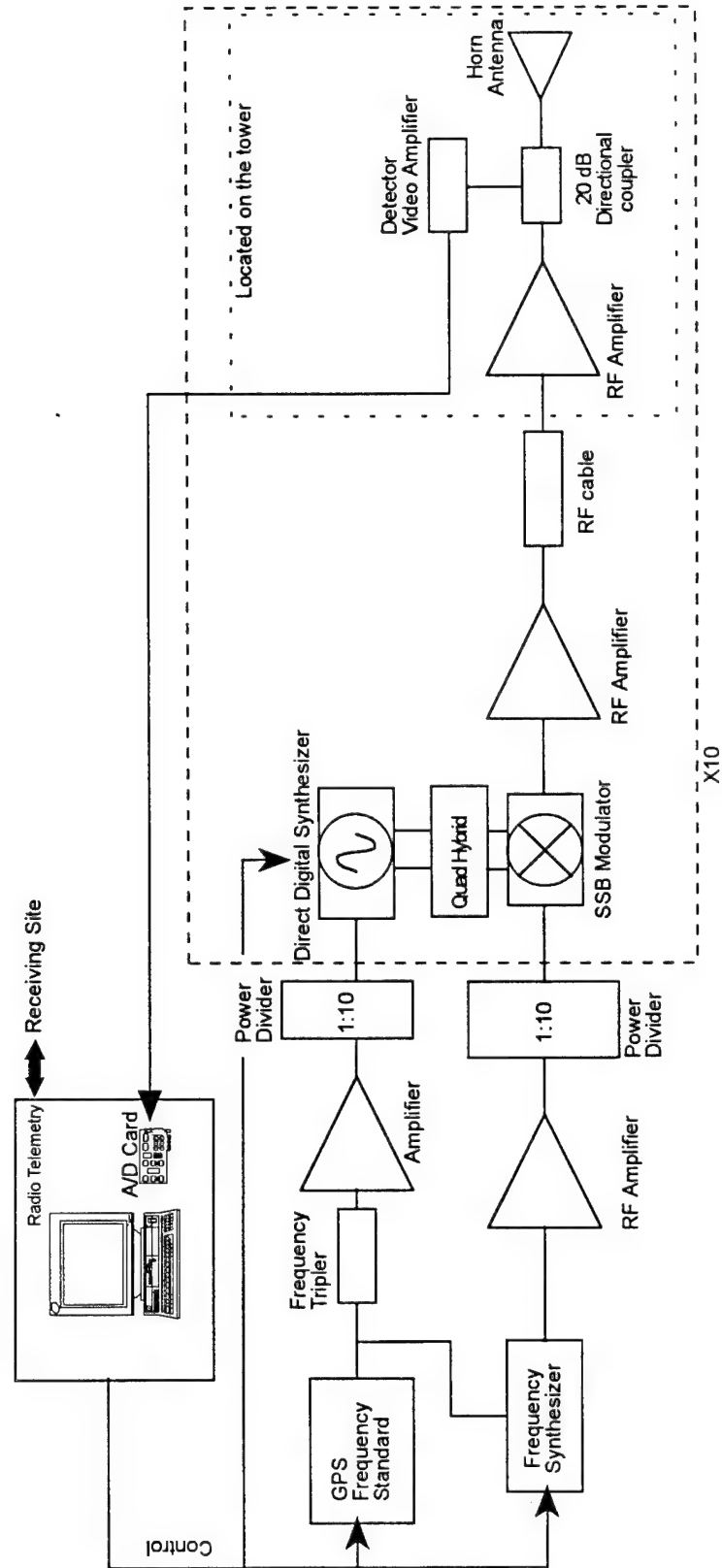


FIGURE A-1. WIDEBAND SYSTEM TRANSMITTER BLOCK DIAGRAM

The receive base station, which serves as the system's primary control, communicates with the transmit site through a radio telemetry link that sets up the transmit parameters, enables or disables each transmit module, and initiates or stops data collection. The receive base station also executes the required signal processing functions using a 486 PC interfaced to two high-speed A/D cards and an ALACRON i860 digital signal processing (DSP) board. The A/D cards can simultaneously sample both the In-phase (I) and Quadrature (Q) channels from all receive modules at a rate of 25 kHz. (Only the I data channel is currently used because of a hardware problem on the A/D boards having to do with interleaving the channels. Thus, the signal-frequency space is effectively halved and the signal-to-noise ratio reduced by 3 dB. Since the transmit signals easily fit in 12.5 kHz and the system has good signal-to-noise performance, the reduction in capability was not considered overly detrimental to the data collection effort.) The A/D data are transferred to the DSP card for execution of Fast Fourier Transforms (FFTs) to analyze the spectral content of the input signal; i.e., separate the received data by transmitter height.

As stated earlier, the system has four receiver modules which are mounted on the 100-ft tower at various heights. Figure A-2 shows a block diagram of the receiver module and base station hardware. Each receiver module first passes the received signal through a digitally tuned YIG bandpass filter. This filter, which has a 30 to 80 MHz bandwidth, acts as a preselector to protect against any interference signals and further reduce the unwanted sideband created by the single-sideband (SSB) mixer. The 3-dB point for each filter was measured at different transmit frequencies and operating temperatures to create a look-up table which is used to calibrate the YIG filter tuning across ambient temperature changes. Following the YIG filter, the RF signal level is passed through a low noise amplifier (LNA) and down-converted to the intermediate frequency (IF). The local oscillator (LO) signal from the system frequency synthesizer is set 100 MHz below the transmitted frequencies to create the IF frequency of 100 MHz. An IF bandpass filter with 2-MHz bandwidth eliminates any unwanted mixing products. To increase the dynamic range of the receiver, a digital attenuator is used before any IF signal amplification. The attenuation is selectable between 0 and 35 dB in 5-dB increments. The IF signal is passed down the tower to the receiver base station where it is down-converted again to baseband (0 to 12.5 kHz for I channel operation only) and ready for processing.

The A/D card simultaneously samples all four receiver signals (I data channel only) and passes that data over to the DSP board. The DSP board is capable of a maximum FFT size of 4096. One of the many possible signal processing options that was used frequently during data collection is described as follows: The DSP board takes 512 data samples and zero-pads to 2048, applies a Hanning weight, and executes an FFT. The FFT output is then averaged with 14 other FFTs accruing from shifting by 256 data samples per step for 50 percent data overlap. The program then searches for the peak signal levels in ten 300-Hz windows centered at the location of each transmitter DDS offset in the baseband spectrum. The received peak signal levels are adjusted by the calibrated receiver gain and then displayed relative to the free-space loss values. The peak signal levels along with the calibration data, the telemetered transmitter power monitor values, and other collection parameters are recorded on a high-density 8-mm tape. An 8-min collection at 2-Hz switching rate followed by a 2-min dead-time interval creates a data file 560 KB in size. Each 8-mm tape is capable of recording for more than 2 weeks around the clock for such a collection interval.

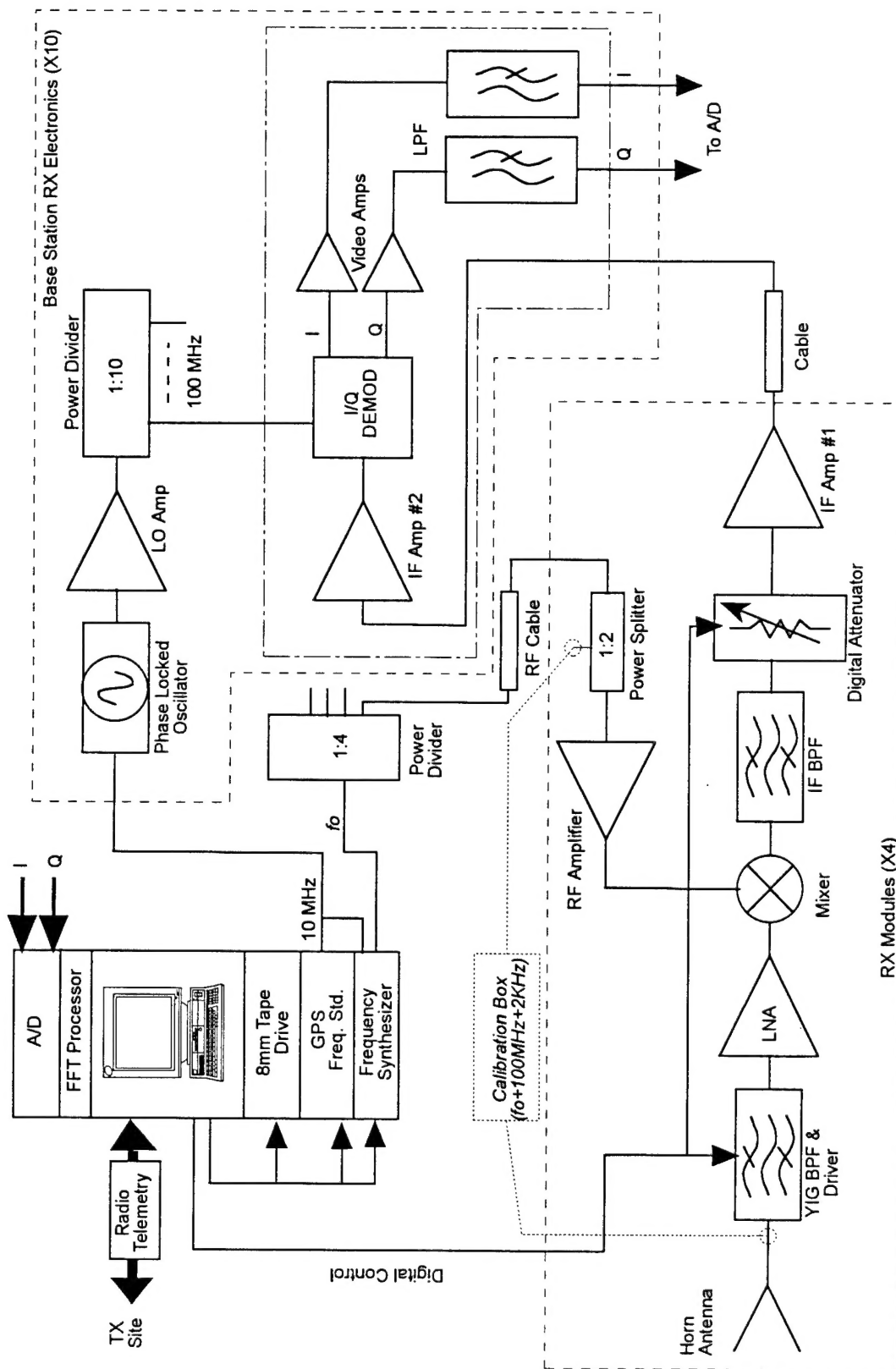


FIGURE A-2. WIDEBAND SYSTEM RECEIVER BLOCK DIAGRAM

During the data collection process, the transmit frequencies are switched at a fixed rate. The receive station must sample and process the received signal, store processed output and telemetered information, and tune to the next transmit frequency at the same rate. Thus it is critical that the receive and transmit stations are synchronized accurately. This accuracy is accomplished using a GPS receiver at both the transmit and receive base stations as the event-trigger source and as the 5-MHz reference-frequency source. When the receiver base station sends a command to the transmit station via the telemetry link to start the collection process at a specified time, both GPS receivers send a triggering pulse when that time is reached. Then they trigger again to change frequencies and process the signal at the specified interval. The 5-MHz oscillator in the GPS receivers is disciplined via the received GPS data at both locations so that the frequency sources at both locations will be locked with a frequency accuracy of  $10^{-11}$  and short-term stability of  $10^{-12}$ . Table A-1 shows the MPMS system parameters.

TABLE A-1. MPMS SYSTEM PARAMETERS

Simultaneous Paths	40 (10 Transmitters , 4 Receivers)
Waveform	CW
Frequency	2-18 GHz
Transmit Power	0.1 W
Antenna	2-18 GHz ridged horns
Antenna Gain	7.9/11.7/8.4 dB (2/10/18 GHz)
Antenna Beamwidth	45 to 9 deg
Height Resolution	Transmitter: 3 ft Receiver: 15 ft*
Receiver Bandwidth	RF: 30 to 80 MHz IF: 2 MHz
A/D Conversion	12 bits @ 25 kHz
FFT	4096 point maximum
Noise Figure	10 dB (includes 4-dB YIG filter loss)
Free Space Signal-to-Noise Ratio** at 10 nmi	2 GHz: 62.6 dB 18 GHz: 47.6 dB

\* Positionable

\*\* Using only real signal and 512 points

**DISTRIBUTION**

	<u>Copies</u>		<u>Copies</u>
<b>DOD ACTIVITIES (CONUS)</b>		ATTN CODE N865	1
ATTN CODE E29L		OFFICE OF THE CHIEF OF NAVAL	
(TECHNICAL LIBRARY)	1	OPERATIONS	
COMMANDING OFFICER		THE PENTAGON RM 4C510	
CSSDD NSWC		DEPARTMENT OF THE NAVY	
6703 W HIGHWAY 98		WASHINGTON DC 20350-2000	
PANAMA CITY FL 32407-7001		ATTN JOE WILLIAMS	1
		TOM HARDY	1
ATTN CODE 5300 MERRILL SKOLNIK	1	COMMANDER	
CODE 5301 G V TRUNK	1	NAVAL SEA SYSTEMS COMMAND	
CODE 5312 PAUL HUGHES	1	2531 JEFFERSON DAVIS HWY	
NAVAL RESEARCH LABORATORY		ARLINGTON VA 22242-5160	
4555 OVERLOOK AVENUE SW			
WASHINGTON DC 20375-5320		ATTN CAPT FRANCIS WILLIAMSON	
		PEO(TAD)D2	1
ATTN CODE 543 R PAULUS	1	PROGRAM EXECUTIVE OFFICER FOR	
CODE 543 H HITNEY	1	THEATER AIR DEFENSE	
CODE 543 K ANDERSON	1	2531 JEFFERSON DAVIS HIGHWAY	
NCCOSC RDTE DIV 543		ARLINGTON VA 22242-5170	
COMMANDING OFFICER			
53170 WOODWARD ROAD		<b>NON-DOD ACTIVITIES (CONUS)</b>	
SAN DIEGO CA 92152-7385		ATTN D DOCKERY	1
ATTN CODE ONR 31 BILL MICELI	1	J PATRICK REILLY	1
CODE ONR 31 JIM HALL	1	J GOLDBIRSH	1
CODE ONR 31 MAX YODER	1	JOHNS HOPKINS UNIVERSITY	
CODE ONR 35 DAVE SIEGEL	1	APPLIED PHYSICS LABORATORY	
CODE ONR 35 ELI ZIMET	1	JOHNS HOPKINS ROAD	
CODE ONR 32		LAUREL MD 20723-6099	
CDR SCOTT SANDGATHE	1		
CODE ONR 32 DAVE JOHNSON	1	ATTN J A SAFFOLD	1
CODE ONR 32 WAYNE PATTERSON	1	GEORGIA TECH RESEARCH INSTITUTE	
CODE ONR 321 DICK DOOLITTLE	1	GEORGIA INSTITUTE OF TECHNOLOGY	
OFFICE OF NAVAL RESEARCH		RADAR SYSTEMS APPLICATIONS	
800 N QUINCY STREET		LABORATORY	
ARLINGTON VA 22217-5660		ATLANTA GA 30332	
DEFENSE TECHNICAL INFORMATION CTR		THE CNA CORPORATION	
CAMERON STATION		PO BOX 16268	
ALEXANDRIA VA 22304-6145	12	ALEXANDRIA VA 22302-0268	1

**DISTRIBUTION (Continued)**

	<u>Copies</u>		<u>Copies</u>
ATTN P MCCRAY	1	F04	1
HUGHES MISSILE SYSTEMS COMPANY		F10	1
BLDG 842 MS 1		F10	1
P O BOX 11337		F102	1
TUCSON AZ 85734-1337		F20	1
		F30	1
ATTN R PAGE	1	F40	1
HUGHES MISSILE SYSTEMS COMPANY		F405	1
BLDG 842 MS 3		F406	1
P O BOX 11337		F41	1
TUCSON AZ 85704		F41	1
		F41	1
ATTN L TAYLOR	1	F41	5
HUGHES MISSILE SYSTEMS COMPANY		F41	1
BLDG 842 MS 9		F41	1
P O BOX 11337		F41	1
TUCSON AZ 85734-1337		F41	1
		F41	1
ATTN DR MATTHEW VANDERHILL	1	F41	1
MIT LINCOLN LABORATORY		F41	1
244 WOOD STREET		F41	1
LEXINGTON MA 02173-9108		F42	1
		F42	1
ATTN EARL H JOHNSON	1	F42	1
MARTIN MARIETTA		F42	1
GOVERNMENT ELECTRONIC SYSTEMS		F42	1
199 BORTON LANDING ROAD		F42	20
POST OFFICE BOX 1027		F42	1
MOORESTOWN NJ 08057-0927		F44	1
		F44	1
ATTN GIFT AND EXCHANGE DIVISION	4	F44	1
LIBRARY OF CONGRESS		F44	1
WASHINGTON DC 20540		F44	1
		F50	1
<b>NON-DOD ACTIVITIES (EX-CONUS)</b>		N24	1
		N742	1
ATTN KENNETH H CRAIG	1		
SIGNAL SCIENCE LTD			
20 ALEXANDER CLOSE			
ABINGDON OXON OX14 1XA UK			

**INTERNAL**

B05	STATON	1
E231		3
E282	SWANSBURG	1
F		1